Stem Cell Reports
Article

ISSCR

OPEN ACCESS

Renal Subcapsular Transplantation of PSC-Derived Kidney Organoids Induces Neo-vasculogenesis and Significant Glomerular and Tubular Maturation *In Vivo*

Cathelijne W. van den Berg,[1,2,*] Laila Ritsma,[3] M. Cristina Avramut,[4] Loes E. Wiersma,[1,2] Bernard M. van den Berg,[1,2] Daniëlle G. Leuning,[1,2] Ellen Lievers,[1,2] Marije Koning,[1,2] Jessica M. Vanslambrouck,[5] Abraham J. Koster,[4] Sara E. Howden,[5,7] Minoru Takasato,[5,6] Melissa H. Little,[5,7] and Ton J. Rabelink[1,2]

[1]Department of Internal Medicine - Nephrology, Leiden University Medical Center, Albinusdreef 2, 2333 ZA Leiden, the Netherlands
[2]Einthoven Laboratory of Vascular and Regenerative Medicine, Leiden University Medical Center, Albinusdreef 2, 2333 ZA Leiden, the Netherlands
[3]Department of Cell and Chemical Biology, Cancer Genomics Centre Netherlands, Leiden University Medical Center, Einthovenweg 20, 2333 ZC Leiden, the Netherlands
[4]Department of Cell and Chemical Biology, Leiden University Medical Center, Einthovenweg 20, 2333 ZC Leiden, the Netherlands
[5]Murdoch Children's Research Institute, Flemington Road, Parkville, VIC 3052, Australia
[6]RIKEN Center for Developmental Biology, Chuou-ku, Kobe 650-0045, Japan
[7]Department of Paediatrics, University of Melbourne, Parkville, VIC 3010, Australia
*Correspondence: c.w.van_den_berg@lumc.nl
https://doi.org/10.1016/j.stemcr.2018.01.041

SUMMARY

Human pluripotent stem cell (hPSC)-derived kidney organoids may facilitate disease modeling and the generation of tissue for renal replacement. Long-term application, however, will require transferability between hPSC lines and significant improvements in organ maturation. A key question is whether time or a patent vasculature is required for ongoing morphogenesis. Here, we show that hPSC-derived kidney organoids, derived in fully defined medium conditions and in the absence of any exogenous vascular endothelial growth factor, develop host-derived vascularization. *In vivo* imaging of organoids under the kidney capsule confirms functional glomerular perfusion as well as connection to pre-existing vascular networks in the organoids. Wide-field electron microscopy demonstrates that transplantation results in formation of a glomerular basement membrane, fenestrated endothelial cells, and podocyte foot processes. Furthermore, compared with non-transplanted organoids, polarization and segmental specialization of tubular epithelium are observed. These data demonstrate that functional vascularization is required for progressive morphogenesis of human kidney organoids.

INTRODUCTION

The adult kidney is a highly complex organ, containing more than 20 specialized cell types, arranged in a spatial architecture critical to its function. Each human kidney contains approximately one million functional units: the nephrons. These regulate the plasma composition by glomerular filtration, active tubular secretion, and reabsorption of waste products and useful substances, respectively, in addition to the contribution of metabolic, hemodynamic, and endocrine functions. Worldwide, the number of patients with end-stage kidney disease necessitating dialysis or transplantation is reaching epidemic proportions (Hill et al., 2016). Therefore, innovative models that can advance our understanding of kidney disease and the potential for endogenous kidney regeneration are warranted. Human pluripotent stem cells (hPSCs) represent one possible source for such replacement kidney tissue.

Human kidney cell types have recently been generated from hPSCs (Freedman et al., 2015; Morizane et al., 2015; Taguchi et al., 2014; Takasato et al., 2015; Xia et al., 2013), and strategies to control and guide the resulting development of these hPSC-derived kidney tissues will be crucial for future regenerative medicine applications. Each of the available protocols varies slightly in the growth factors used, timing, and format of cell culture. As such, each protocol generates slightly different subsets of renal cell types (Morizane and Bonventre, 2017). Xia et al. (2013) generated ureteric bud progenitor cells that contribute to the collecting duct after co-culture with embryonic kidney, while Taguchi et al. (2014), working first with mouse embryonic stem cells, showed the exclusive induction of nephrons with strong evidence for podocyte formation. This group has subsequently provided a separate protocol for the generation of collecting duct from mouse PSC (Taguchi and Nishinakamura, 2017). Takasato et al. developed a differentiation protocol that simultaneously induces all four renal progenitors (nephron progenitors, ureteric bud progenitors, renal interstitial progenitors, and endothelial progenitors) from human induced pluripotent stem cells (hiPSCs) to generate what are referred to as kidney organoids (Takasato et al., 2015, 2016). In these human kidney organoids, segmented nephrons are connected to collecting ducts, surrounded by renal interstitial cells and an endothelial network (Takasato et al., 2015, 2016). While this and some other protocols (Freedman et al., 2015) show evidence for the formation of a vasculature, not all protocols contain endothelial cells (Morizane et al., 2015) and, when vascular tissue is present,

peritubular and glomerular capillary beds are not yet appropriately patterned (Freedman et al., 2015; Takasato et al., 2015). Although each of these approaches can generate cell types and structures recognizable as elements of a developing human kidney, they represent protocols spanning no more than a few weeks of culture. As such, the degree of resulting maturation *in vitro* is universally low, as demonstrated at the transcriptional and morphological level, while the anatomical structure is also inaccurate. This raises the question of whether maturation requires additional time, changes in culture conditions or a patent blood supply.

The formation of the glomerulus in mice commences with the involution of the proximal end of the elongating nephron to form an outer layer of parietal epithelial cells and an internal group of pre-podocytes (Quaggin and Kreidberg, 2008). This occurs without an apparent need for inductive signals from mesangial cells or the vascular endothelium. However, development of a glomerular filtration barrier and formation of slit diaphragms is known to require the presence of vascularization (Quaggin and Kreidberg, 2008). In the embryonic mouse kidney, SCL^+ progenitors have been shown to be essential in initiating the development of the glomerular microcirculation with the FOXD1-derived stroma giving rise to all mural populations with these being essential for appropriate vascular patterning (Dekel et al., 2003, 2004; Sequeira-Lopez et al., 2015; Sequeira Lopez and Gomez, 2011). While these progenitor populations are present in the developing organ, the major blood vessels are thought to arise via angiogenic ingrowth from outside of the developing organ (Dekel et al., 2003). Multiple studies have shown that, upon transplantation of embryonic human and mouse kidney tissue *in vivo*, vascular precursors within the transplanted tissue can give rise to the glomerular capillaries (donor-derived vasculogenesis), but also that host-derived endothelial cells can migrate into the graft to form blood vessels within the transplant (Dekel et al., 1997, 2002; Hammerman, 2004; Rogers et al., 1998). Sharmin et al. (2016) showed evidence for vascularization and podocyte slit diaphragm formation in hPSC-derived kidney structures treated with vascular endothelial growth factor (VEGF) and placed under the renal capsule of recipient mice. However, the differentiation protocol used in that study contained predominantly nascent glomeruli and little proximal tubular structures. In contrast, the protocol of Takasato et al. (2015) already showed evidence of capillary loop stage glomerular maturation *in vitro* due to the presence of an hPSC-derived endothelial cell population. However, while endothelium was present in this study, vascular flow was not and glomerular vascular ingrowth was uncommon.

In the current study, we have modified the kidney organoid differentiation protocol of Takasato et al. (2015, 2016) for application with hPSC lines derived or adapted to maintenance culture in feeder-free Essential 8 (E8)-defined medium (Chen et al., 2011). We have then compared the degree of glomerular, tubular, and vascular maturation across time between organoids after renal subcapsular transplantation in the absence of any supporting growth factors versus organoids after continued culture *in vitro*. Using immunofluorescence, unbiased wide-field nano-electron microscopy and *in vivo* imaging, we show evidence for substantial glomerular, tubular, and vascular maturation only in the presence of a patent functional vasculature.

RESULTS

Feeder-free Maintenance and Seeding of hPSCs in E8 Medium

The kidney organoid differentiation protocol of Takasato et al. (2015, 2016) was developed using pluripotent stem cell lines derived and maintained on mouse embryonic feeders (MEFs). As the field moves to feeder-free culture systems, this may affect transferability of the protocol between different hPSC lines and different laboratories. Hence we first investigated the possibility of generating kidney organoids from hPSCs that were maintained in E8 medium. To optimize seeding of the cells for the start of the differentiation, we compared various dissociation reagents, extracellular matrices, addition of a supplement and cell density (Figure S1). Cells were initially cultured on MEFs and adapted to culture in E8 medium using EDTA (Figure S1A) or were derived in E7 medium without the use of MEFs (Figure S2A). Differentiation was performed on either vitronectin or Matrigel, with morphology more reproducible on vitronectin (Figure S1B). Cell confluency at commencement of differentiation was very important. Passaging the hPSCs with EDTA resulted in the formation of small clumps, making precise seeding of cell numbers difficult resulting in lower-differentiation reproducibility. We therefore switched our cultures to dissociation with TrypLE Select, which provided the opportunity to passage the hPSCs as single cells. However, survival of these cells post dissociation was very low and we therefore supplemented the medium with RevitaCell, a commercially available Rho-kinase inhibitor, for 24 hr after plating, which substantially increased survival and attachment of the cells (Figure S1C). We were now able to plate a more precise and reproducible number of cells per well for the differentiation. We next investigated a range of 5,000–20,000 cells/cm^2 (Figure S1D). Differentiations that were initially seeded in E8 medium at a density of 10,000 cells/cm^2 using TrypLE Select with RevitaCell on vitronectin were highly reproducible with high differentiation

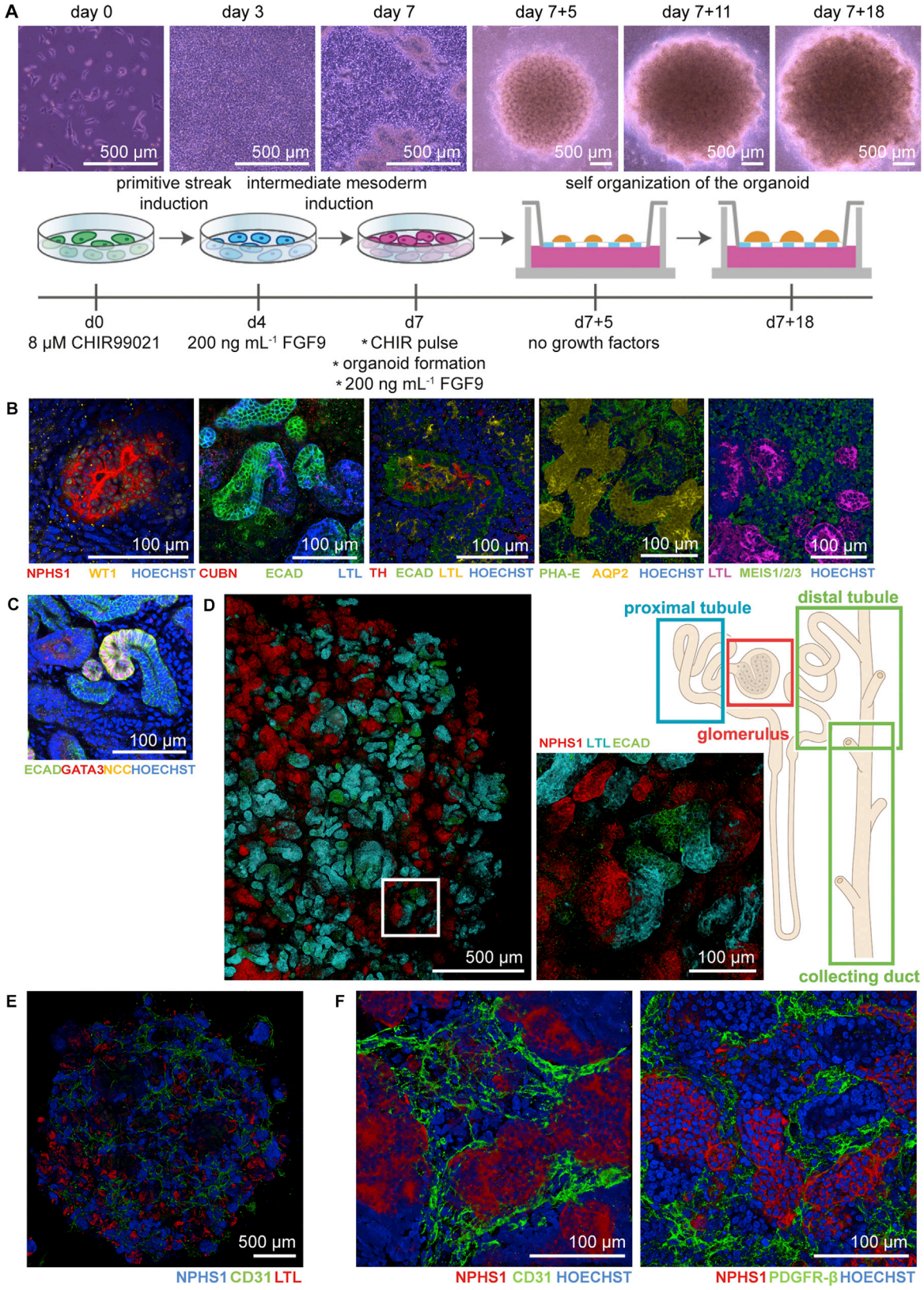

(legend on next page)

efficiency and all further experiments were therefore performed using these conditions (Figure S1E). Results were obtained and reproduced in six different hPSC lines, including hiPSC-CRL1502 (clone C32) that was used for the original Takasato paper (Takasato et al., 2015), as well as human embryonic stem cell (hESC) line hES3 ENVY (Costa et al., 2005), hiPSC lines LUMC0072iCTRL01, LUMC0099iCTRL04, and two reporter hPSC lines hiPSC *MAFB*:mTagBFP2 (hiPSC-MAFB-BFP) (Howden et al., unpublished data) marking podocytes and H9 hESC line *SOX17*$^{mCHERRY/w}$*RUNX1C*$^{GFP/w}$ (hESC-SOX17-mCherry) (Ng et al., 2016) marking endothelial cells.

Kidney Organoids Develop Completely Formed Nephron Structures

As described previously (Takasato et al., 2016), hPSCs were differentiated as a monolayer by activating WNT-signalling using CHIR99021 for 4 days followed by FGF9 and heparin to induce the simultaneous formation of ureteric epithelium with the metanephric mesenchyme. On day 7, the cells were pulsed with CHIR99021 before dissociation, aggregation, and transfer to transwell filters to form 3D structures and continued to differentiate supported by the air-liquid interface. On day 7 + 5, FGF9 and heparin were removed from the medium and nephrogenesis was visualized by the formation of small vesicles in the organoids (Figure 1A). To evaluate the outcome, organoids were cultured until day 7 + 18 of differentiation, and characterized for the presence of appropriate structures using immunofluorescence. NPHS1 and WT1 marked the podocytes in the glomerular structures (Figure 1B). Furthermore, proximal tubular (CUBN$^+$, PHA-E$^+$, LTL$^+$), loop of Henle (Tamm-Horsfall$^+$), distal tubular (ECAD$^+$, GATA3$^-$), collecting duct (ECAD$^+$, GATA3$^+$, AQP2$^+$) structures, and interstitial cells (MEIS1/2/3$^+$) were identified (Figure 1B). Successful differentiation was observed in six independent cell lines (four hiPSCs and two hESCs) (Figures S2B and S2C). We also show the presence of the sodium chloride co-transporter (NCC) on both the basolateral and apical membrane of the distal convoluted tubule cells (Figure 1C). Whole organoid immunofluorescence showed the presence of appropriately segmenting nephron structures with glomeruli (NPHS1$^+$), proximal tubule (LTL$^+$), and distal tubule/collecting duct (ECAD$^+$) (Figure 1D). As previously reported, day 7 + 18 kidney organoids contained NPHS1$^+$ glomerular structures surrounded by CD31$^+$ endothelial cells and PDGFR-β$^+$ pericytes (Figures 1E and 1F). However, formation of the capillary loop inside the glomerular structures was not overtly evident.

Organized Glomerular and Tubular Structures Observed by Electron Microscopy

To further evaluate the organization and maturity of the glomerular and tubular structures, we performed both scanning and transmission electron microscopy (SEM, TEM) analysis of organoids at day 7 + 18. SEM showed a glomerular structure in the organoid that was surrounded by a putative Bowman's capsule. The podocytes inside the Bowman's capsule were aligned and showed small, immature foot processes (Figure S3A). To allow for an unbiased assessment of ultrastructural features of the organoids, we used tiling of adjacent TEM fields to produce virtual slides providing a wide field of view at nanometer-scale resolution (Faas et al., 2012). Such unbiased wide-field nanomicroscopy revealed the presence of primitive foot processes in between the glomerular cells (Figures 2A and 2B). At this time point, the tubular structures were multilayered epithelial structures with no or a small lumen, with some evidence of apical microvilli forming (Figures 2A, 2B, and S3B). In addition, mitochondria were present in these cells. The multi-layered or pseudo-stratified epithelium, and the lack of a clear tubular basement membrane, suggested incomplete polarization. As suggested by the immunofluorescence, there was no evidence of glomerular vasculature in these organoids.

Prolonged Time in Culture Does Not Influence Organoid Maturation

To evaluate the influence of prolonged culture on these kidney organoids, we evaluated the organoids after 7 + 53 days in culture on the air-liquid interface using nanomicroscopy. We observed lack of evidence for glomerular

Figure 1. Kidney Organoids Derived from Induced Pluripotent Stem Cells Display Structures Characteristic of a Nephron on Day 7 + 18 of Differentiation

(A) Bright-field images and schematic of the experimental time line for the generation of kidney organoids.

(B) Immunofluorescence analysis of the different segments of the nephron: podocytes (WT1$^+$, NPHS1$^+$), proximal tubule (CUBN$^+$, PHA-E$^+$, LTL$^+$), Lis of Henle (Tamm Horsfall$^+$), distal tubule (ECAD$^+$), collecting duct (AQP-2$^+$), and stromal cells (MEIS1/2/3$^+$) visualized as 3D structures.

(C) Presence of the sodium chloride (NCC) symporter in the kidney organoid.

(D) Tile scan of an immunofluorescent organoid demonstrating anatomically correct interconnected segments of the nephron: glomerulus, proximal tubule, distal tubule, and collecting duct. Close-up view of the boxed area displays the structures in detail.

(E) Endothelial cells (CD31$^+$) are mainly localized around glomerular structures (NPHS1$^+$) and not around tubular structures (LTL$^+$).

(F) The CD31$^+$ cells do not invade glomerular structures (NPHS1$^+$) and pericytes (PDGFR-β$^+$) surround glomerular structures.

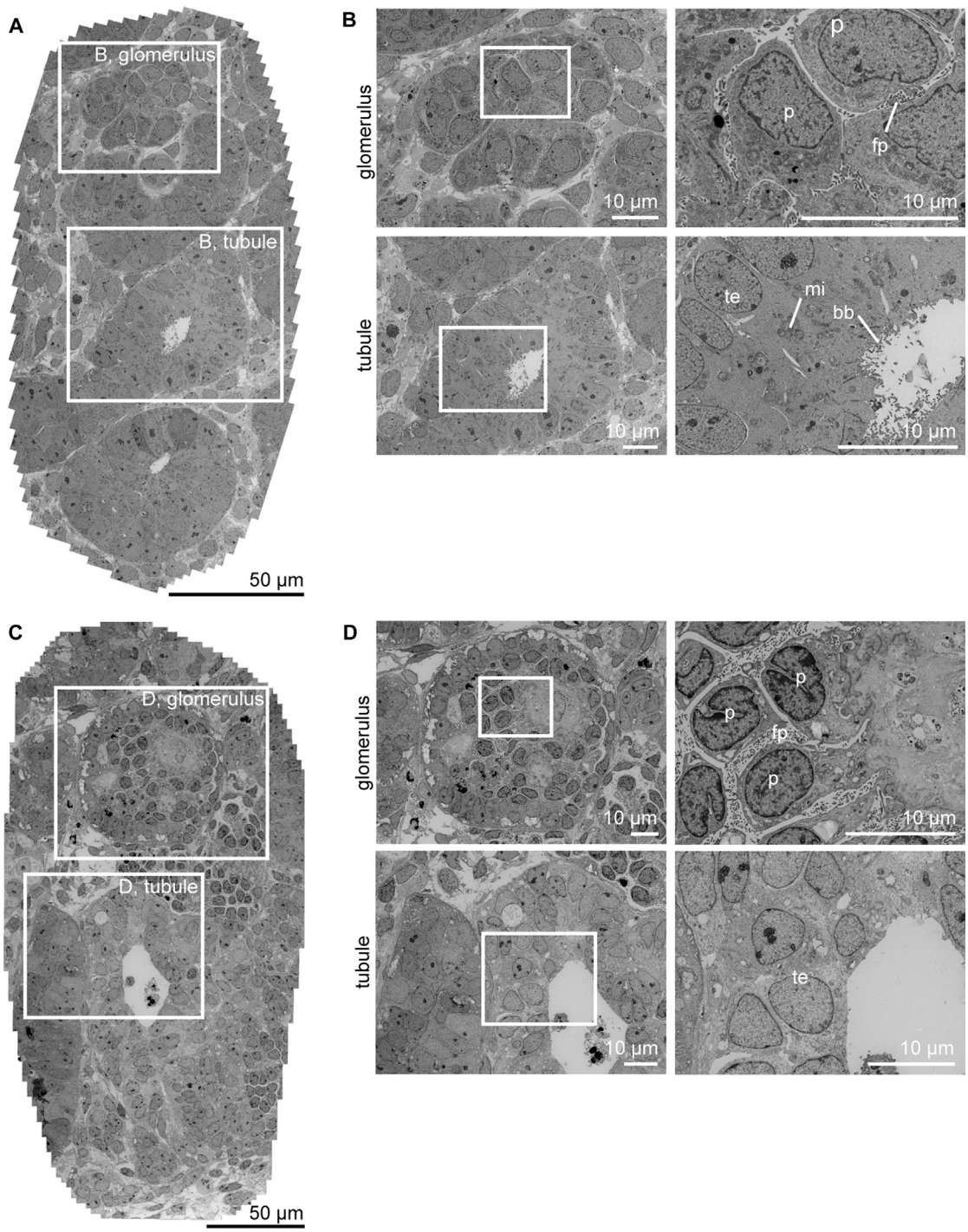

Figure 2. Ultrastructural Evaluation Shows Lack of Advanced Maturation of Kidney Organoids *In Vitro* over Time at Day 7 + 18 and Day 7 + 53

(A) Low-magnification transmission electron microscopy (TEM) tile scan of kidney organoid cultured for 7 + 18 days on the air-liquid interface displaying glomerular and tubular structures.

(B) High-magnification TEM images of boxed areas in (A) demonstrate characteristic structures, such as podocytes with primitive foot processes in glomerulus (top) and brush border with microvilli in the open lumen of a tubular structure (bottom).

(C) Low-magnification TEM image of a kidney organoid cultured for prolonged time (7 + 53 days) on the air-liquid interface.

(legend continued on next page)

capillaries, extraglomerular podocytes, and substantial deposition of glomerular extracellular matrix, little evidence of tubular maturation, the presence of ectopic stromal tissues, and cell death (Figures 2C and 2D). We focused on the presence of CD31$^+$ cells in the organoids after prolonged culture and observed progressive loss of these cells around day 7 + 25 (data not shown). This is consistent with our previous profiling of the differentiation protocol where vascular gene expression decreased between 7 + 11 and 7 + 18 days (Takasato et al., 2015). One possible cause for a lack of robust vascularization of these developing glomeruli would be the absence of VEGF production by the podocytes. We therefore evaluated the production of VEGF by these organoids and found increased VEGF levels across time in culture, peaking by day 7 + 17 and remaining at this level even after culture for 7 + 52 days (Figure 3A). Given the evidence for VEGF production within the kidney organoids, it was possible that even more prolonged time in culture may have been required for increased instances of capillary loop formation *in vitro*. The immature phenotype of the tubules may also have reflected insufficient time for tubular elongation and segment differentiation. However, we conclude that prolonged culture in this format does not facilitate onward differentiation of kidney organoids, whereas, likely due to the large size of these structures, a progressive pathology arises resulting from hypoxia and metabolic deficit.

Kidney Organoids Become Functionally Vascularized upon Transplantation *In Vivo*

As has been studied previously with transplantation of human and mouse metanephric tissues (Dekel et al., 2002, 2003, 1997; Hammerman, 2004), we aimed to examine the degree of organoid maturation achieved upon transplantation under the renal capsule of recipient immunocompromised mice. Bisected day 7 + 18 kidney organoids were transplanted under the renal capsule for up to 28 days. The size of the organoid increased progressively with time of transplantation (Figure 3B), and toluidine blue staining demonstrated presence of glomerular and tubular structures within the organoid after transplantation (Figure 3C). SEM analysis suggests the presence of vasculature inside the organoid and the glomerular structures (Figure 3D). Indeed, host-derived mouse endothelial cells (MECA-32$^+$) were evident within the hiPSC-derived transplanted organoid (Figure 3E). Further analysis on the location of mouse endothelial cells, showed an invasion of host cells inside glomerular-like structures (NPHS1$^+$ and WT1$^+$) (Figure 3F). In addition, we observed peritubular vascularization in association with tubular epithelium (Figure 3G).

To study functionality of the vasculature we used repeated intravital multiphoton imaging of the neo-vascularized transplanted organoids. We employed the combinatorial approach of organoid transplantation and an abdominal imaging window (AIW) (Ritsma et al., 2012) to serially image the transplanted organoids *in vivo* through imaging windows that were surgically implanted in the flank of the animal (Figure 4A). Kidney organoids (day 7 + 18) were generated using our previously described reporter hiPSC line in which blue fluorescent protein (mTAG-BFP) was inserted into one copy of the *MAFB* gene, a transcription factor expressed in the podocytes of the glomerulus (Howden et al., unpublished data). *In vitro*, this results in the clear co-localization of BFP and the glomerular-expressed protein NPHS1 (Figure S4A). These iPSC-MAFB-BFP kidney organoids were bisected and transplanted under the renal capsule of the left kidney of recipient mice. Immediately afterward, the kidney was secured in the subcutaneous space by tightening the abdominal muscle tissue around the kidney stalk without restricting the vascular flow. The AIW was implanted in the skin on top of the kidney. At both day 7 and 14 after transplantation, mice were intravenously injected with 2,000 kDa fluorescein isothiocyanate (FITC)-labelled dextran just prior to imaging to visualize host-derived blood flow. Intravital imaging revealed the presence of host-derived blood flow (FITC-labelled dextran, green) through glomerular structures (MAFB-BFP, blue) within the organoids (Figures 4B–4E; Movie S1). To test whether the hPSC-derived endogenous vascular plexus present within the transplanted organoids connects to the invading host vasculature, similar experiments were performed using transplanted organoids derived from the hESC-SOX17-mCherry reporter line (Ng et al., 2016). This allowed us to visualize the organoid-derived mCherry$^+$ endothelial cells (Figure S4B).

In contrast to the loss of endothelial cells in organoids maintained in culture, we noted that the pre-existing human vascular plexus in the organoids was still present after the transplantation procedure (Figures 4F and 4G). Using intravital microscopy we showed that part of this human-derived vascular plexus was perfused by the injected FITC-labelled dextran, suggesting that the plexus functionally connects to the ingrowing host-derived renal vasculature (Figure 4F; Movie S2). Indeed, immunofluorescence

(D) Detailed TEM images of boxed areas in (C) from glomerular structure (top) and tubular structure (bottom) demonstrate features of maturation, such as foot processes, formation of glomerular basement membrane, and microvilli, respectively. However, the structures are more disorganized.

p, podocyte; fp, foot processes; te, tubular epithelium; mi, mitochondria; bb, brush border.

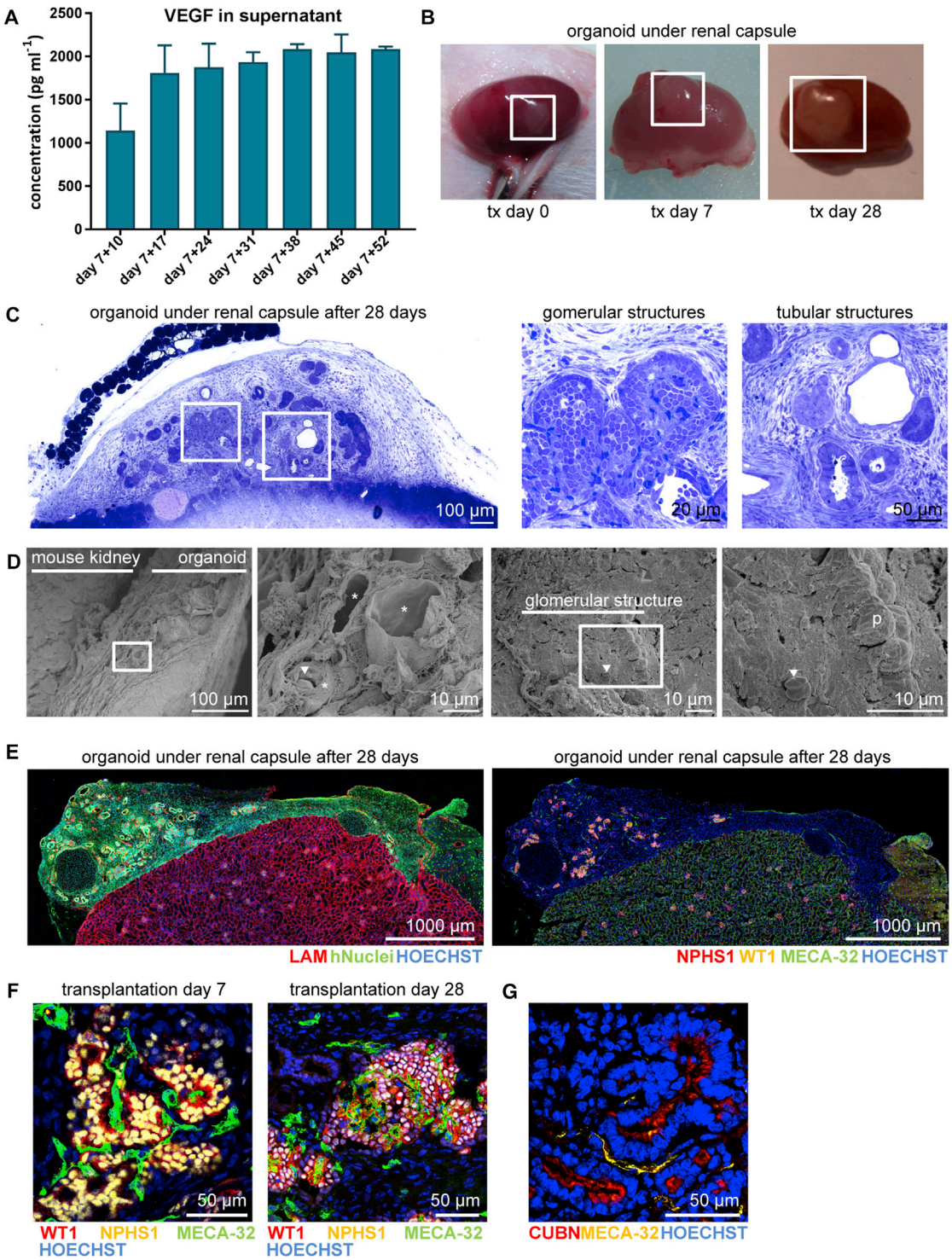

Figure 3. Kidney Organoids Become Vascularized upon Transplantation for 7 and 28 Days

(A) Concentration of VEGF (pg mL^{-1}) determined by Luminex assay in the supernatant of three cultured organoids measured weekly from day 7 + 10 until day 7 + 52. Data are represented as means ± SEM.

(B) Transplanted human kidney organoid under renal capsule of mice on the day of transplantation (tx), after 7 and 28 days showing growth upon vascularization.

(legend continued on next page)

showed the combined presence of human CD31$^+$ and mouse MECA-32$^+$ endothelial cells in these organoids at transplantation day 14 (Figure 4G), showing the contribution from both host and donor to the vascular network.

Kidney Organoids Mature Progressively with Time of Transplantation

After 7 days of perfusion there is already fenestrated, specialized endothelium, and the initial deposition of a glomerular basement membrane (GBM) present within transplanted organoids (Figure 5A). Secondary to this phenomenon, primitive podocytes are aligned to the GBM and show apical-to-basal migration of tight junctions, as was described during podocyte maturation in the capillary loop stage of glomerulogenesis (Kim et al., 2017). After prolonged perfusion at day 28 of transplantation, the podocytes spread out along the basement membrane with basal adherens junctions near a clear trilaminar GBM, indicating progression toward the formation of slit diaphragms between podocyte foot processes (asterisk, Figure 5B). Of note, this organized GBM is lacking in the organoids that were not transplanted (Figure 2). Such extensive evidence of maturation post transplantation of organoids is very promising, even when compared with the GBM, fenestrated endothelium, and mature podocyte structures within an adult kidney (Figure S5A).

Tubular structures within transplanted organoids also displayed progressive maturation across time after transplantation, resulting in polarization of the epithelium into a single monolayer and the formation of regions of well-developed apical brush border (Figures 6A and 6B). Furthermore, tubular lumina widened progressively and peritubular capillaries were aligning the tubules (Figure 7A), such as in the human kidney (Figure S5B). In addition, signs of apico-basal polarization could be observed, such as the presence of luminal microvilli and cilia (Figure 7B). After 28 days of transplantation, ultrastructural evidence of intratubular specification was also suggested by the presence of intercalated cells, characterized by a high number of mitochondria and micro projections (Figure 7B) (Roy et al., 2015), with these cells representing a hallmark of the collecting duct in the adult kidney.

DISCUSSION

In this study, we have directly compared the effect of prolonged *in vitro* culture versus transplantation on the forward maturation of hPSC-derived organoids. We show the development of a functional host-derived vascular network that invades the developing glomerular structures in the organoids upon transplantation. With time, transplantation resulted in progressive maturation of the glomerular filtration barrier together with the deposition of a GBM, the development of fenestrated glomerular endothelium, and apical-basal polarization of the podocytes. Time-matched non-transplanted organoids do not show any of these phenomena, but remain structurally immature and disorganized. Similarly, with time post transplantation, tubular epithelial maturation is observed with the development of a polarized single-layer epithelium, widened lumina with areas that display an extensive brush border, as can be seen in proximal tubules, and areas with intratubular segmental specification, such as can be observed in the collecting duct in the adult kidney.

These experiments establishing the capacity of a PSC-derived model of the human kidney recapitulate earlier work by Dekel et al. (2003) and Harari-Steinberg et al. (2013), where human fetal kidney tissue was transplanted under the kidney capsule. In the work of Dekel et al., early fetal, but not mature, human kidney tissue was able to recruit host-derived endothelial cells to form a host-derived glomerular circulation (Dekel et al., 2003). Here we show that the vascular network originating from the hPSC lines and present within the organoids contribute to graft vascularization via anastomosis to the host-derived endothelial plexus. This appears to recapitulate the embryonic development of the kidney vasculature, where both angiogenic hemangioblast precursor cells, as well as vasculogenic endothelial precursors within the organ itself, are required for development of the glomerular microcirculation (Halt et al., 2016; Robert et al., 1998; Sequeira Lopez and Gomez, 2011). To explore whether the pre-existing vascular network in the organoids connects to the ingrowing host circulation, we transplanted organoids derived from hESC-SOX17-mCherry under the kidney capsule, thus

(C) Toluidine blue staining of organoid under the renal capsule after 28 days of transplantation. Boxed areas highlight glomerular and tubular structures displayed on the right.
(D) Scanning electron microscopy images suggests blood vessels in the kidney organoid after transplantation and inside a glomerular structure. Close-up views of boxed areas are displayed.
(E) Immunofluorescent overview of human nuclei and LAMININ (LAM) in the organoid under the renal capsule of a mouse kidney (left) and integration of mouse endothelial cells (MECA-32$^+$) in the organoid and glomerular structures (right).
(F) Mouse endothelial cells (MECA-32$^+$) were observed in association with glomerular structures (NPHS1$^+$, WT1$^+$) in the human kidney organoid after 7 and 28 days of transplantation.
(G) Peritubular vascularization observed as MECA-32$^+$ endothelial cells aligning tubular (CUBN$^+$) structures.
p, podocyte; arrowhead, erythrocyte; asterisk, blood vessels.

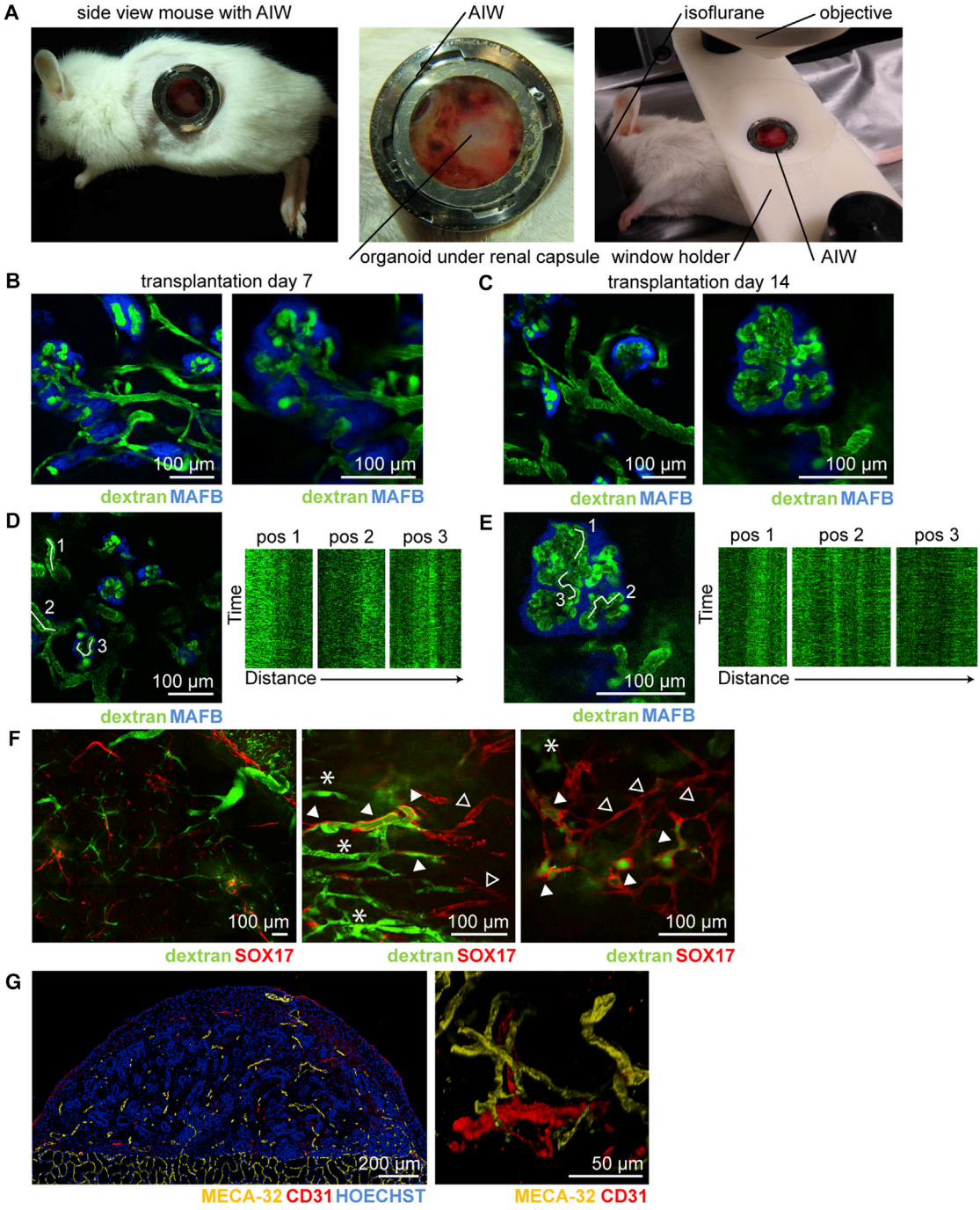

Figure 4. *In Vivo* Imaging of Vascularized Kidney Organoids Shows Glomerular Vascularization and Chimeric Organoid Circulation after 7 and 14 Days of Transplantation

(A) Mouse with the abdominal imaging window (AIW) on the left kidney and a close-up view of a kidney window after 14 days of implantation. Right picture shows the mouse with the AIW installed for microscope analysis.

(B and C) *In vivo* imaging of transplanted organoids derived from hiPSC-MAFB-BFP after 7 days (B) and 14 days (C) of transplantation. Circulating plasma was visualized with 2,000 kDa FITC-labelled dextran and flow was detected in BFP^+ glomerular structures.

(D and E) Kymographs from marked positions demonstrating the dynamic blood flow through the capillary in the organoid (D) and inside the glomerular structure (E) after 14 days of transplantation.

(legend continued on next page)

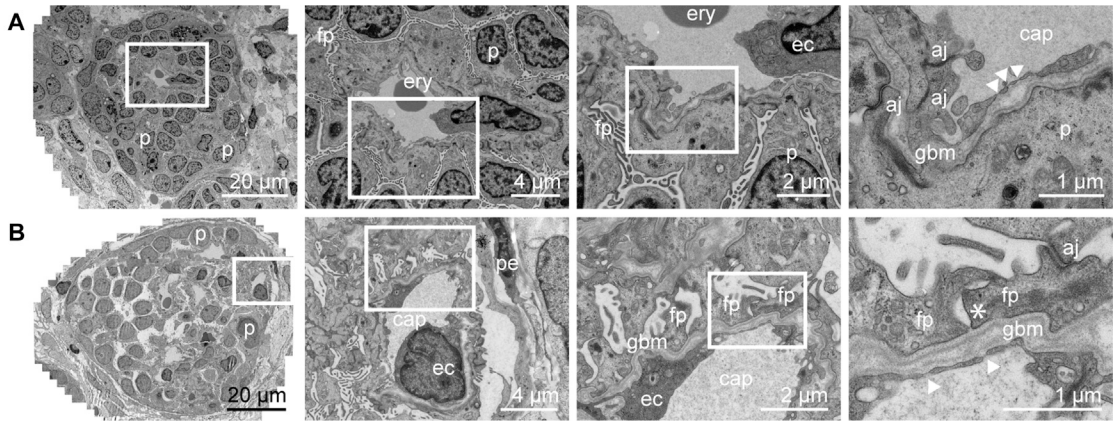

Figure 5. Wide-Field Ultrastructural Evaluation of Transplanted Organoids Shows Evidence for Glomerular Vascularization and Maturation

Transmission electron micrographs of vascularized glomerular structures after 7 days (A) and 28 days (B) of transplantation. Glomeruli become organized displaying features of maturation such as foot processes, formation of glomerular basement membrane and progression toward the formation of a slit diaphragm. Close-up views of the boxed areas are displayed.

p, podocyte; fp, foot processes; ery, erythrocyte; ec, endothelial cell; aj, adherens junctions; gbm, glomerular basement membrane; arrowhead, endothelial fenestrae; cap, capillary; pe, parietal epithelium; asterisk, developing slit diaphragm.

allowing fate mapping of donor-derived endothelium. Our results show that there is still a SOX17-mCherry$^+$ vascular network present in the kidney organoids for at least 14 days after transplantation. Part of this network becomes connected to the host circulation upon transplantation, as indicated by the dextran-FITC perfusion, which underscores the vasculogenic potential of this plexus. The apparent lack of ingrowth of the pre-existing vascular network into glomeruli of the cultured organoids may to some extent reflect a culture condition less permissive for vasculogenic activity within organoids. On the other hand, podocytes were shown to produce high amounts of VEGF, even after prolonged *in vitro* culture in APEL medium, which should have facilitated endothelial cell migration into the glomerular structures. Our data suggest that angiogenic ingrowth from the host was either required to drive vasculogenesis of the endogenous endothelium in the kidney organoids or simply facilitated the survival of these cells.

It is well known that both the formation of the GBM as well as the attainment of the fenestrated endothelial phenotype depend upon iterative growth factor cross-communication between podocytes and endothelial precursor cells (Quaggin and Kreidberg, 2008). This process is critical to the development of a functioning glomerular filtration unit (Scott and Quaggin, 2015), and the subsequent developmental organization of the kidney. The ultrastructural analysis of the glomerular filtration barrier in the transplanted organoids shows an advanced state of maturation and is indicative of functional endothelial-podocyte crosstalk. The peritubular microcirculation primarily derives from the efferent arteriole of the glomerular capillary network (Sequeira Lopez and Gomez, 2011). After organoid transplantation, host-derived peritubular capillaries were also observed particularly at 28 days of transplantation, whereas the CD31$^+$ cells that were originally present in the organoids did not show such an organization. This further indicates the progressive development of a renal microcirculatory network.

Previous studies using human and mouse PSC-derived nephrons (Sharmin et al., 2016; Taguchi et al., 2014) demonstrated vascularization of iPSC-derived podocytes upon transplantation under the kidney capsule. The model developed by Sharmin et al. however, used a distinct differentiation protocol (Taguchi et al., 2014), which generates significant evidence of glomerular/proximal nephron segments, but appears to lack more distal nephron cell types. Their transplantation approach also required the addition of VEGF to the transplant and resulted in excessive growth of non-renal stromal cells during prolonged transplantation. In this study, we show that the kidney organoids themselves actively secrete VEGF and did not require any

(F) Low and high magnification of hESC-SOX17-mCherry derived kidney organoids after transplantation for 14 days revealing mCherry$^+$ endothelial cells perfused with FITC-labelled dextran (arrowhead) and host-derived vasculature (asterisk). Note that not all mCherry$^+$ endothelial cells were perfused (open arrowhead).

(G) Immunofluorescence of human CD31$^+$ and mouse MECA-32$^+$ in the transplanted kidney organoid.

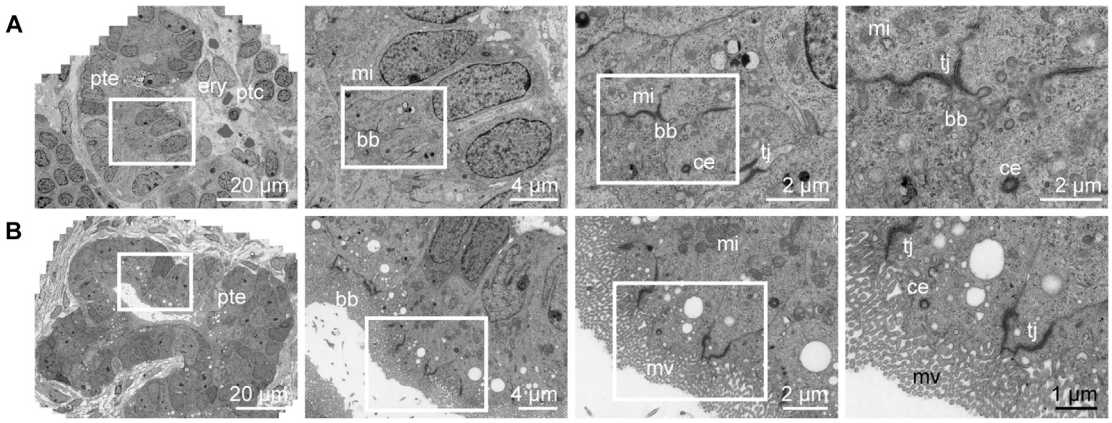

Figure 6. Wide-Field Ultrastructural Evaluation of Transplanted Organoids Shows Advanced Tubular Epithelial Differentiation

Transmission electron micrographs of developing tubular structure with peritubular capillaries after 7 days (A) and 28 days (B) of transplantation under the renal capsule. After transplantation, the tubular structures display a single layer of epithelial cells connected with tight junctions, have an open lumen and show tubular polarization, such as characteristic mitochondria, microvilli, and centrioles. Close-up views of the boxed areas are displayed.

pte, proximal tubular epithelium; ptc, peritubular capillary; ery, erythrocyte; mi, mitochondria; bb, brush border; tj, tight junction; ce, centriole; mv, microvilli.

further stimulation to induce host-derived angiogenic vascularization upon transplantation.

To date, a substantial amount of published kidney organoid characterization has been performed at the level of immunofluorescence. It is important to note that, while this approach can identify the presence of protein markers for various renal segments from early on, the apparent presence of these markers remained present even in long-term *in vitro* cultures and have not been useful as markers for maturation. To assess tissue and cellular maturation in this study, we used virtual nanomicroscopy (Faas et al., 2012), an approach that employs TEM, rapid automated data collection, and stitching, to create large virtual slides with a relatively large field of view at nanometer-scale resolution. Having access to data at this scale and resolution allows for a genuine and unbiased representation of ultrastructural events at the level of several nephron structures. The virtual nanomicroscopy approach allowed for assessment of maturation by ultrastructural mapping of cellular processes, such as apicobasal polarization of epithelium and the formation and structure of the glomerular filtration barrier.

It is possible that the prolonged *in vitro* culture of kidney organoids in the current format (floating filter at an air-liquid interface) was unsuccessful at supporting maturation for reasons other than a lack of blood flow. By day 7 + 25, kidney organoids are 5–7 mm in diameter and potentially reaching a size unsupported by the culture system itself.

While changes to the *in vitro* culture approach may improve outcomes, it would appear that the capacity to visualize a perfused transplanted organoid *in vivo* using the abdominal window approach may provide a far superior approach to evaluating progress *in vivo*. Indeed, this may be a notable approach for disease modeling where maturation of appropriate tubular compartments is likely to be crucial.

We also demonstrate here the feasibility of transferring the existing protocol by Takasato et al. (2016) from hPSCs cultured on feeders to E8 culture such that both the culture of the undifferentiated hiPSCs and the differentiation procedure itself are fully defined and serum free. Despite these changes, this protocol resulted in highly reproducible and efficient differentiations from multiple starting cell lines and did not compromise the potential to derive all renal progenitor lineages. This revised protocol will enhance the broad utility of kidney organoids by increasing the transferability between different hPSC lines and different laboratories.

In summary, kidney organoids may provide a suitable technology for drug screening, disease modeling, and studying kidney regeneration. Most of the current developments in this field are still solely focused on kidney (proximal) tubular epithelial cells. However, renal toxicity can also primarily occur in the glomerulus (Barri et al., 2004; Musu et al., 2011; Naesens et al., 2009; Semeniuk-Wojtas et al., 2016). Nephrotoxic drugs such as bisphosphonates, cyclosporine, NSAIDs, antihypertensive drugs, and anti-angiogenesis inhibitors have been shown to predominantly lead to glomerulopathies by compromising endothelial-podocyte crosstalk or podocyte integrity (Radhakrishnan and Perazella, 2015). Similarly,

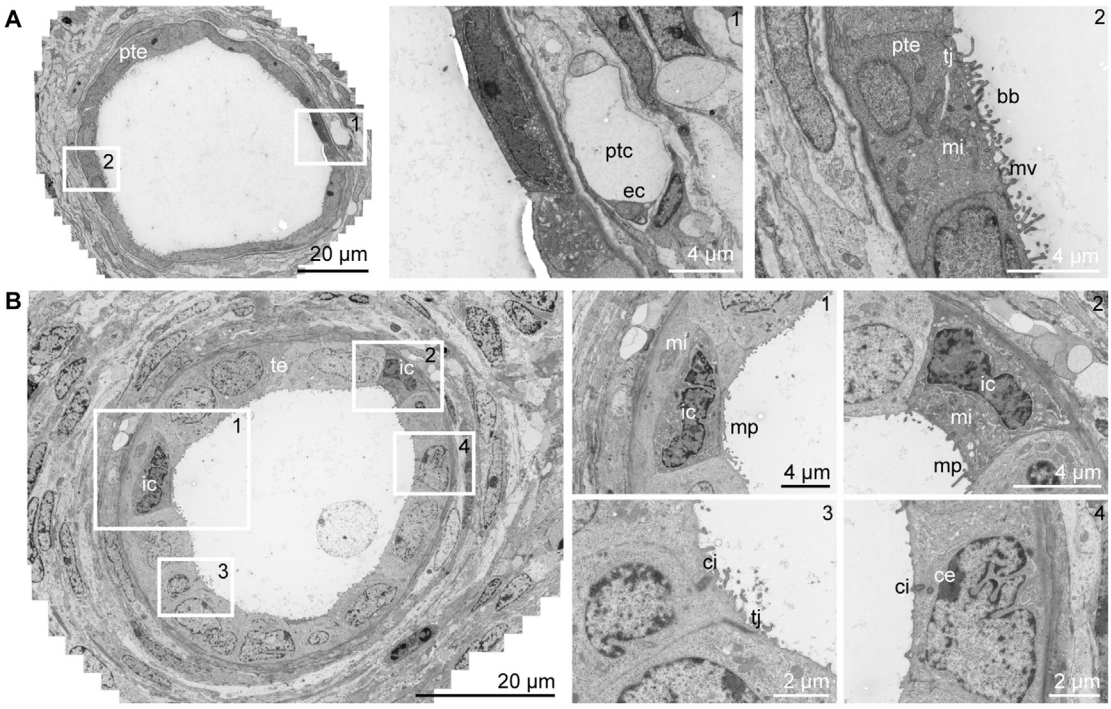

Figure 7. Wide-Field Ultrastructural Evaluation of Transplanted Organoids Demonstrates Peritubular Vascularization and Intratubular Specification

(A) Transmission electron microscopy stitch showing tubular structures after 28 days of transplantation displaying an open lumen with a single layer of epithelial cells. The tubule has a brush border, tight junctions, and a peritubular capillary.

(B) Transmission electron micrographs showing tubular dilation with micro projections that suggest the presence of intercalated cells existing in the collecting duct-type structure.

Boxed areas correspond with numbered close-up views. te, tubular epithelium, ptc, peritubular capillary; bb, brush border; ec, endothelial cell; tj, tight junction; ic, intercalated cell; ci, cilium; ce, centriole; mv, microvilli; mi, mitochondria; mp, micro projections.

most kidney diseases are primarily glomerulus-associated diseases. The vascularized kidney organoids, and in particular the potential to develop a glomerular filtration unit in these organoids, may constitute a more faithful model for screening of nephrotoxicity, as well as renal disease modeling.

EXPERIMENTAL PROCEDURES

Full details are provided in Supplemental Experimental Procedures.

Maintenance of hPSCs

hESC and hiPSC lines were transferred to culture on vitronectin in E8 medium (Thermo Fisher Scientific) and maintained for several passages as small clumps using 0.5 mM UltraPure EDTA (Thermo Fisher Scientific) before transfer to culture as single cells using TrypLE Select (Thermo Fisher Scientific) and the addition RevitaCell Supplement (Thermo Fisher Scientific) for 24 hr.

hESC-ENVY (Costa et al., 2005), H9 hESC line *SOX17*$^{mCHERRY/w}$ *RUNX1C*$^{GFP/w}$ (hESC-SOX17-mCherry) (Ng et al., 2016), and hiPSC-CRL1502 clone C32 (Briggs et al., 2013) were initially maintained on irradiated MEFs in hESC medium (Costa et al., 2008). An extra hiPSC-CRL1502 line was generated without culture on MEFs using episomal reprogramming plasmids (Chen et al., 2011; Howden et al., 2015). Reporter hiPSC *MAFB*:mTagBFP2 (hiPSC-MAFB-BFP) was simultaneously reprogrammed and gene-edited using CRISPR/Cas9 (Howden et al., unpublished data). LUMC0072iCTRL01 and LUMC0099iCTRL04 were generated on MEFs from fibroblasts using a Simplicon RNA Reprogramming Kit (Millipore) (iPSC core facility, LUMC) and further cultured in TeSR-E8 medium (Stem Cell Technologies).

Differentiation and Organoid Formation

hPSCs were plated on vitronectin-coated culture dishes at 10,000 cells/cm^2 in E8 medium supplemented with RevitaCell. The differentiation was started (day 0) when the dish was 10%–20% confluent (usually 24 hr). Cells were incubated for 4 days in 8 μM CHIR99021 (R&D Systems) in STEMdiff APEL medium (APEL). On day 4 medium was switched to APEL medium containing 200 ng mL^{-1} rhFGF9 (R&D Systems) and 1 μg mL^{-1} heparin (Sigma-Aldrich). Cells were switched (day 7) from monolayer culture to 3D culture on Transwell 0.4 μM pore polyester membranes

in the same medium after a 1 hr pulse with 5 μM CHIR. On day 7 + 5, growth factors were removed and APEL medium was changed every 2 days. Organoids were maintained on the transwell membranes until day 7 + 18 to day 7 + 53.

Animal Experiments

All animal experimental protocols were approved by the animal welfare committee of the Leiden University Medical Center. Recipient mice (n = 8, non-obese diabetic/severe combined immunodeficiency, 8 weeks, Charles River Laboratories) were anesthetized with isoflurane and injected with temgesic (buprenorphine) for pain relief. Core body temperature was maintained at 37°C. Via flank incisions, the kidneys were exteriorized and a small incision was made in the renal capsule. Kidney organoids (day 7 + 18) were bisected and transplanted under renal capsule of both kidneys. Samples were collected after 7 and 28 days.

Intravital Microscopy

For intravital microscopy, hiPSC-MAFB-BFP and hESC-SOX17-mCherry organoids were transplanted (n = 10), and a titanium AIW was implanted on top of the left kidney as described previously (Ritsma et al., 2012; van Gurp et al., 2016). Seven and 14 days after surgery, mice were intravitally imaged on a Zeiss LSM 710 NLO upright multiphoton microscope equipped with a Mai Tai Deep See multiphoton laser (690–1040 nm). Mice were injected in the tail vein with 2,000 kDa FITC-Dextran (100 μL of 20 mg/mL, Sigma FD2000S) and were placed on their side on a custom-made microscope insert with the window stably fixed in an upward horizontal position using a custom made window holder. Imaging was performed through a W Plan-Apochromat 20×/1.0 DIC M27 75 mm objective. Fluorophores in iPSC-MAFB-BFP organoids were excited at 800 nm and emission was collected in two LSM PMTs: FITC (522–600 nm) and BFP (440–500 nm). Fluorophores in hESC-SOX17-mCherry organoids were excited using single photon at 488 (FITC) and 568 (mCherry), and emission was collected in two LSM PMTs: FITC (500–558 nm) and mCherry (578–700 nm). Time-lapse series were collected and Z stacks were taken with a Z step of 1 or 2 μm.

Immunohistochemistry

Organoids were stained for kidney structures as described previously (Takasato et al., 2015, 2016). Organoids under the mouse renal capsule were snapfrozen in TissueTek or fixed in 2% paraformaldehyde and stored in PBS. Mouse on Mouse Basic Kit was used to detect structures in the transplanted human organoid and mouse kidney. Tissues were examined using the White Light Laser Confocal Microscope TCS SP8 using LAS-X Image software with 3D module (Leica) or the LSM 780 confocal microscope (Zeiss).

Cytokine Analysis

Cell culture supernatant of the organoids was collected weekly from day 7 + 10 until day 7 + 52 from 1 to 3 wells with 3 organoids during 3 independent differentiations. The levels of VEGF were assessed using the Human Premixed Magnatic Luminex Assay for VEGF. The Bio-Plex Luminex system (Bio-Rad) was used for readout and VEGF concentration was expressed as pg mL^{-1}.

TEM and SEM

Tissue samples of organoids and organoids under the mouse renal capsule were analyzed for TEM at an acceleration voltage of 120 kV using an FEI Tecnai 12 (BioTWIN) transmission electron microscope (FEI), equipped with an FEI 4k Eagle CCD camera. Virtual slides showing glomerular and tubular structures were recorded using automated large-scale data acquisition combined with stitching software (Faas et al., 2012). Images were captured at 13,000× or 18,500× magnification, respectively, corresponding to a 1.66 or 1.22 nm pixel size at the specimen level. For SEM, images were acquired on a JEOL JSM-6700F Field Emission Scanning Electron Microscope (JEOL Europe).

SUPPLEMENTAL INFORMATION

Supplemental Information includes Supplemental Experimental Procedures, five figures, and two movies and can be found with this article online at https://doi.org/10.1016/j.stemcr.2018.01.041.

AUTHOR CONTRIBUTIONS

C.W.v.d.B. designed and performed experiments, analyzed and interpreted data, and wrote the manuscript. L.R., M.C.A., L.E.W., B.M.v.d.B., D.G.L., E.L., M.K., and J.M.V. performed experiments and acquired and/or interpreted data. S.E.H generated and characterized reporter lines, acquired data, and interpreted data. A.J.K. facilitated electron microscopy research. M.T. provided advice and contributed intellectually. T.J.R. and M.H.L. designed experiments, interpreted data, and wrote the manuscript.

ACKNOWLEDGMENTS

We thank Christian Freund (hiPSC core facility, LUMC, Leiden, the Netherlands) for providing two hiPSC lines (LUMC0072iCTRL01 and LUMC0099iCTRL04), Christine Mummery (LUMC, Leiden, the Netherlands) for providing hES3 ENVY, and Andrew Elefanty and Edouard Stanley (MCRI, Melbourne, Australia) for providing reporter hESC-SOX17-mCherry. We acknowledge the support of Maaike Hanegraaf, Angela Koudijs, Dorien Ward-van Oostwaard, Manon Zuurmond (LUMC, Leiden, the Netherlands), Caro Overmars-Bos and Joost Hoenderop (Radboud UMC, Nijmegen, the Netherlands), and Pei Er, Joanne Soo and Irene Ghobrial (MCRI, Melbourne, Australia). M.H.L. is a Senior Principal Research Fellow of the National Health and Medical Research Council of Australia (GNT1042093). Funding is from the European Community's Seventh Framework Program (FP7/2007-2013) (Stem cell-based therapy for kidney repair, STELLAR, grant agreement number 305436) and RECellularizing ORgan Donors for KIDney bioengineering (RECORD KID, Dutch Kidney Foundation, 15RN02), the NIH (DK107344), and the National Health and Medical Research Council (NHMRC, GNT1100970). C.W.v.d.B. is supported by the Wiyadharma fellowship (Bontius Stichting, LUMC). L.R. is supported by a Veni-grant from the Netherlands Organisation for Scientific Research (NWO, 016.176.081), the Gisela Thier grant (LUMC), and a subsidy from the Leids Universiteits Fonds (LUF, CWB 7204). MCRI is supported by the Victorian Government's Operational Infrastructure Support Program.

Received: June 9, 2017
Revised: January 30, 2018
Accepted: January 30, 2018
Published: March 1, 2018

REFERENCES

Barri, Y.M., Munshi, N.C., Sukumalchantra, S., Abulezz, S.R., Bonsib, S.M., Wallach, J., and Walker, P.D. (2004). Podocyte injury associated glomerulopathies induced by pamidronate. Kidney Int. *65*, 634–641.

Briggs, J.A., Sun, J., Shepherd, J., Ovchinnikov, D.A., Chung, T.L., Nayler, S.P., Kao, L.P., Morrow, C.A., Thakar, N.Y., Soo, S.Y., et al. (2013). Integration-free induced pluripotent stem cells model genetic and neural developmental features of down syndrome etiology. Stem Cells *31*, 467–478.

Chen, G., Gulbranson, D.R., Hou, Z., Bolin, J.M., Ruotti, V., Probasco, M.D., Smuga-Otto, K., Howden, S.E., Diol, N.R., Propson, N.E., et al. (2011). Chemically defined conditions for human iPSC derivation and culture. Nat. Methods *8*, 424–429.

Costa, M., Dottori, M., Ng, E., Hawes, S.M., Sourris, K., Jamshidi, P., Pera, M.F., Elefanty, A.G., and Stanley, E.G. (2005). The hESC line Envy expresses high levels of GFP in all differentiated progeny. Nat. Methods *2*, 259–260.

Costa, M., Sourris, K., Hatzistavrou, T., Elefanty, A.G., and Stanley, E.G. (2008). Expansion of human embryonic stem cells in vitro. Curr. Protoc. Stem Cell Biol. *Chapter 1*, Unit 1C.1.1–1C.1.7.

Dekel, B., Amariglio, N., Kaminski, N., Schwartz, A., Goshen, E., Arditti, F.D., Tsarfaty, I., Passwell, J.H., Reisner, Y., and Rechavi, G. (2002). Engraftment and differentiation of human metanephroi into functional mature nephrons after transplantation into mice is accompanied by a profile of gene expression similar to normal human kidney development. J. Am. Soc. Nephrol. *13*, 977–990.

Dekel, B., Burakova, T., Arditti, F.D., Reich-Zeliger, S., Milstein, O., Aviel-Ronen, S., Rechavi, G., Friedman, N., Kaminski, N., Passwell, J.H., et al. (2003). Human and porcine early kidney precursors as a new source for transplantation. Nat. Med. *9*, 53–60.

Dekel, B., Burakova, T., Ben-Hur, H., Marcus, H., Oren, R., Laufer, J., and Reisner, Y. (1997). Engraftment of human kidney tissue in rat radiation chimera: II. Human fetal kidneys display reduced immunogenicity to adoptively transferred human peripheral blood mononuclear cells and exhibit rapid growth and development. Transplantation *64*, 1550–1558.

Dekel, B., Hochman, E., Sanchez, M.J., Maharshak, N., Amariglio, N., Green, A.R., and Izraeli, S. (2004). Kidney, blood, and endothelium: developmental expression of stem cell leukemia during nephrogenesis. Kidney Int. *65*, 1162–1169.

Faas, F.G., Avramut, M.C., van den Berg, B.M., Mommaas, A.M., Koster, A.J., and Ravelli, R.B. (2012). Virtual nanoscopy: generation of ultra-large high resolution electron microscopy maps. J. Cell Biol. *198*, 457–469.

Freedman, B.S., Brooks, C.R., Lam, A.Q., Fu, H., Morizane, R., Agrawal, V., Saad, A.F., Li, M.K., Hughes, M.R., Werff, R.V., et al. (2015). Modelling kidney disease with CRISPR-mutant kidney organoids derived from human pluripotent epiblast spheroids. Nat. Commun. *6*, 8715.

Halt, K.J., Parssinen, H.E., Junttila, S.M., Saarela, U., Sims-Lucas, S., Koivunen, P., Myllyharju, J., Quaggin, S., Skovorodkin, I.N., and Vainio, S.J. (2016). CD146(+) cells are essential for kidney vasculature development. Kidney Int. *90*, 311–324.

Hammerman, M.R. (2004). Organogenesis of kidneys following transplantation of renal progenitor cells. Transpl. Immunol. *12*, 229–239.

Harari-Steinberg, O., Metsuyanim, S., Omer, D., Gnatek, Y., Gershon, R., Pri-Chen, S., Ozdemir, D.D., Lerenthal, Y., Noiman, T., Ben-Hur, H., et al. (2013). Identification of human nephron progenitors capable of generation of kidney structures and functional repair of chronic renal disease. EMBO Mol. Med. *5*, 1556–1568.

Hill, N.R., Fatoba, S.T., Oke, J.L., Hirst, J.A., O'Callaghan, C.A., Lasserson, D.S., and Hobbs, F.D. (2016). Global prevalence of chronic kidney disease - a systematic review and meta-analysis. PLoS One *11*, e0158765.

Howden, S.E., Maufort, J.P., Duffin, B.M., Elefanty, A.G., Stanley, E.G., and Thomson, J.A. (2015). Simultaneous reprogramming and gene correction of patient fibroblasts. Stem Cell Reports *5*, 1109–1118.

Kim, Y.K., Refaeli, I., Brooks, C.R., Jing, P., Gulieva, R.E., Hughes, M.R., Cruz, N.M., Liu, Y., Churchill, A.J., Wang, Y., et al. (2017). Gene-edited human kidney organoids reveal mechanisms of disease in podocyte development. Stem Cells *35*, 2366–2378.

Morizane, R., and Bonventre, J.V. (2017). Kidney organoids: a translational journey. Trends Mol. Med. *23*, 246–263.

Morizane, R., Lam, A.Q., Freedman, B.S., Kishi, S., Valerius, M.T., and Bonventre, J.V. (2015). Nephron organoids derived from human pluripotent stem cells model kidney development and injury. Nat. Biotechnol. *33*, 1193–1200.

Musu, M., Finco, G., Antonucci, R., Polati, E., Sanna, D., Evangelista, M., Ribuffo, D., Schweiger, V., and Fanos, V. (2011). Acute nephrotoxicity of NSAID from the foetus to the adult. Eur. Rev. Med. Pharmacol. Sci. *15*, 1461–1472.

Naesens, M., Kuypers, D.R., and Sarwal, M. (2009). Calcineurin inhibitor nephrotoxicity. Clin. J. Am. Soc. Nephrol. *4*, 481–508.

Ng, E.S., Azzola, L., Bruveris, F.F., Calvanese, V., Phipson, B., Vlahos, K., Hirst, C., Jokubaitis, V.J., Yu, Q.C., Maksimovic, J., et al. (2016). Differentiation of human embryonic stem cells to HOXA(+) hemogenic vasculature that resembles the aorta-gonad-mesonephros. Nat. Biotechnol. *34*, 1168–1179.

Quaggin, S.E., and Kreidberg, J.A. (2008). Development of the renal glomerulus: good neighbors and good fences. Development *135*, 609–620.

Radhakrishnan, J., and Perazella, M.A. (2015). Drug-induced glomerular disease: attention required!. Clin. J. Am. Soc. Nephrol. *10*, 1287–1290.

Ritsma, L., Steller, E.J., Beerling, E., Loomans, C.J., Zomer, A., Gerlach, C., Vrisekoop, N., Seinstra, D., van Gurp, L., Schafer, R., et al. (2012). Intravital microscopy through an abdominal imaging window reveals a pre-micrometastasis stage during liver metastasis. Sci. Transl. Med. *4*, 158ra145.

Robert, B., St John, P.L., and Abrahamson, D.R. (1998). Direct visualization of renal vascular morphogenesis in Flk1 heterozygous mutant mice. Am. J. Physiol. *275*, F164–F172.

Rogers, S.A., Lowell, J.A., Hammerman, N.A., and Hammerman, M.R. (1998). Transplantation of developing metanephroi into adult rats. Kidney Int. *54*, 27–37.

Roy, A., Al-bataineh, M.M., and Pastor-Soler, N.M. (2015). Collecting duct intercalated cell function and regulation. Clin. J. Am. Soc. Nephrol. *10*, 305–324.

Scott, R.P., and Quaggin, S.E. (2015). Review series: the cell biology of renal filtration. J. Cell Biol. *209*, 199–210.

Semeniuk-Wojtas, A., Lubas, A., Stec, R., Szczylik, C., and Niemczyk, S. (2016). Influence of tyrosine kinase inhibitors on hypertension and nephrotoxicity in metastatic renal cell cancer patients. Int. J. Mol. Sci. *17*, 2073.

Sequeira-Lopez, M.L., Lin, E.E., Li, M., Hu, Y., Sigmund, C.D., and Gomez, R.A. (2015). The earliest metanephric arteriolar progenitors and their role in kidney vascular development. Am. J. Physiol. Regul. Integr. Comp. Physiol. *308*, R138–R149.

Sequeira Lopez, M.L., and Gomez, R.A. (2011). Development of the renal arterioles. J. Am. Soc. Nephrol. *22*, 2156–2165.

Sharmin, S., Taguchi, A., Kaku, Y., Yoshimura, Y., Ohmori, T., Sakuma, T., Mukoyama, M., Yamamoto, T., Kurihara, H., and Nishinakamura, R. (2016). Human induced pluripotent stem cell-derived podocytes mature into vascularized glomeruli upon experimental transplantation. J. Am. Soc. Nephrol. *27*, 1778–1791.

Taguchi, A., Kaku, Y., Ohmori, T., Sharmin, S., Ogawa, M., Sasaki, H., and Nishinakamura, R. (2014). Redefining the in vivo origin of metanephric nephron progenitors enables generation of complex kidney structures from pluripotent stem cells. Cell Stem Cell *14*, 53–67.

Taguchi, A., and Nishinakamura, R. (2017). Higher-order kidney organogenesis from pluripotent stem cells. Cell Stem Cell *21*, 730–746.e6.

Takasato, M., Er, P.X., Chiu, H.S., and Little, M.H. (2016). Generation of kidney organoids from human pluripotent stem cells. Nat. Protoc. *11*, 1681–1692.

Takasato, M., Er, P.X., Chiu, H.S., Maier, B., Baillie, G.J., Ferguson, C., Parton, R.G., Wolvetang, E.J., Roost, M.S., Chuva de Sousa Lopes, S.M., et al. (2015). Kidney organoids from human iPS cells contain multiple lineages and model human nephrogenesis. Nature *526*, 564–568.

van Gurp, L., Loomans, C.J.M., van Krieken, P.P., Dharmadhikari, G., Jansen, E., Ringnalda, F., Beerling, E., van Rheenen, J., and de Koning, E.J.P. (2016). Sequential intravital imaging reveals in vivo dynamics of pancreatic tissue transplanted under the kidney capsule in mice. Diabetologia *59*, 2387–2392.

Xia, Y., Nivet, E., Sancho-Martinez, I., Gallegos, T., Suzuki, K., Okamura, D., Wu, M.Z., Dubova, I., Esteban, C.R., Montserrat, N., et al. (2013). Directed differentiation of human pluripotent cells to ureteric bud kidney progenitor-like cells. Nat. Cell Biol. *15*, 1507–1515.

Stem Cell Reports, Volume *10*

Supplemental Information

Renal Subcapsular Transplantation of PSC-Derived Kidney Organoids Induces Neo-vasculogenesis and Significant Glomerular and Tubular Maturation *In Vivo*

Cathelijne W. van den Berg, Laila Ritsma, M. Cristina Avramut, Loes E. Wiersma, Bernard M. van den Berg, Daniëlle G. Leuning, Ellen Lievers, Marije Koning, Jessica M. Vanslambrouck, Abraham J. Koster, Sara E. Howden, Minoru Takasato, Melissa H. Little, and Ton J. Rabelink

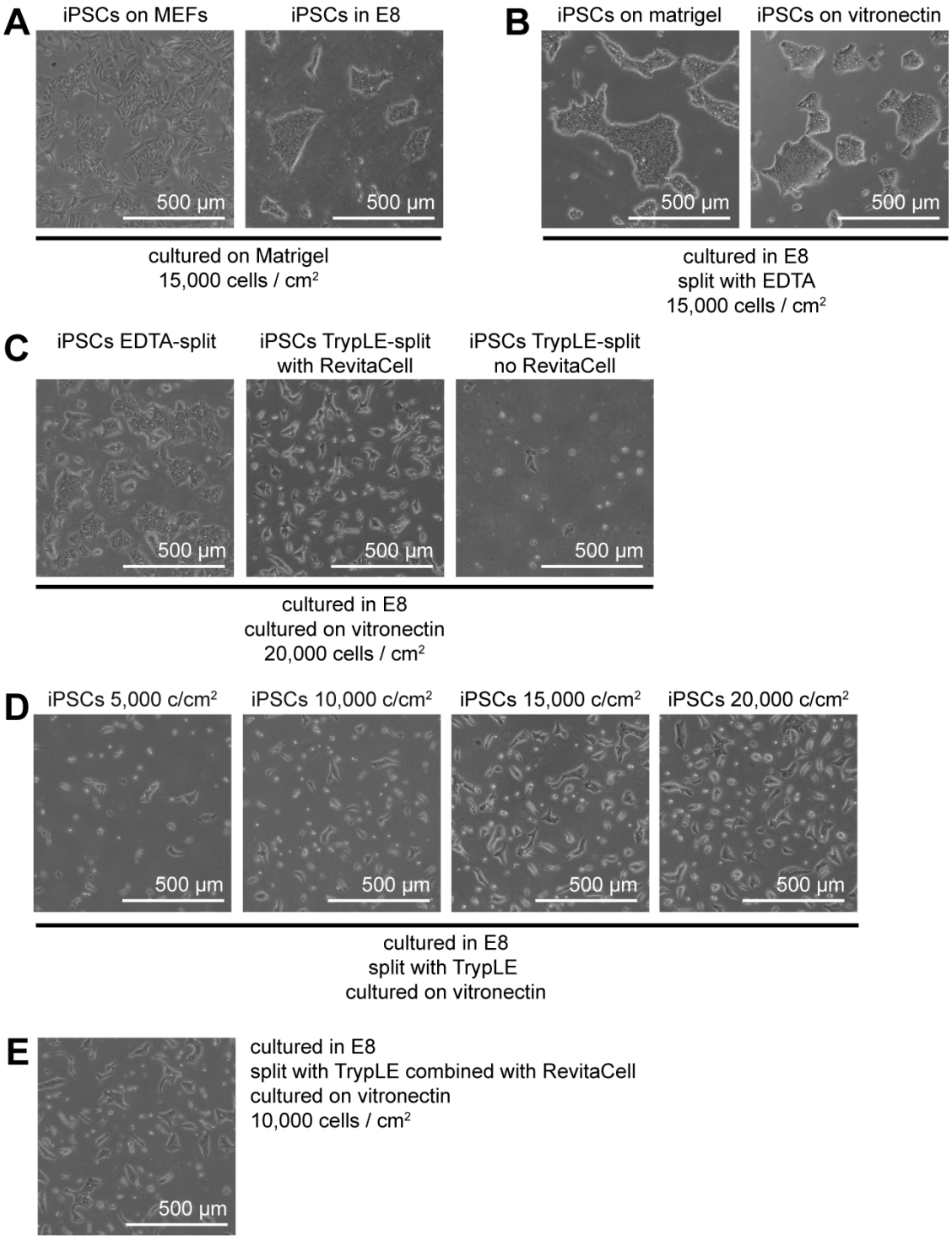

Figure S1: Adaptation of Culture Protocol for Differentiation of Pluripotent Stem Cells to Kidney Organoids using Defined Medium

Numerous variables were investigated for optimal differentiation procedure: **(A)** culture medium, **(B)** matrix, **(C)** passaging reagents, and **(D)** cell density.

(A) Pluripotent stem cells were initially enzymatically passaged on MEFs and were adapted to Essential 8 (E8) cultures. Cells were passaged using EDTA and plated on matrigel using 15,000 cells/cm^2.

(B) Cell matrix was changed from matrigel to more defined vitronectin for better support of differentiation in the early differentiation stages.

(C) Single cell passaging and estimating precise cell numbers is possible using a combination of TrypLE Select and RevitaCell.

(D) Seeding density for pluripotent stem cells was optimized for organoid differentiation.

(E) Final parameters for differentiation of pluripotent stem cells to kidney progenitor cells.

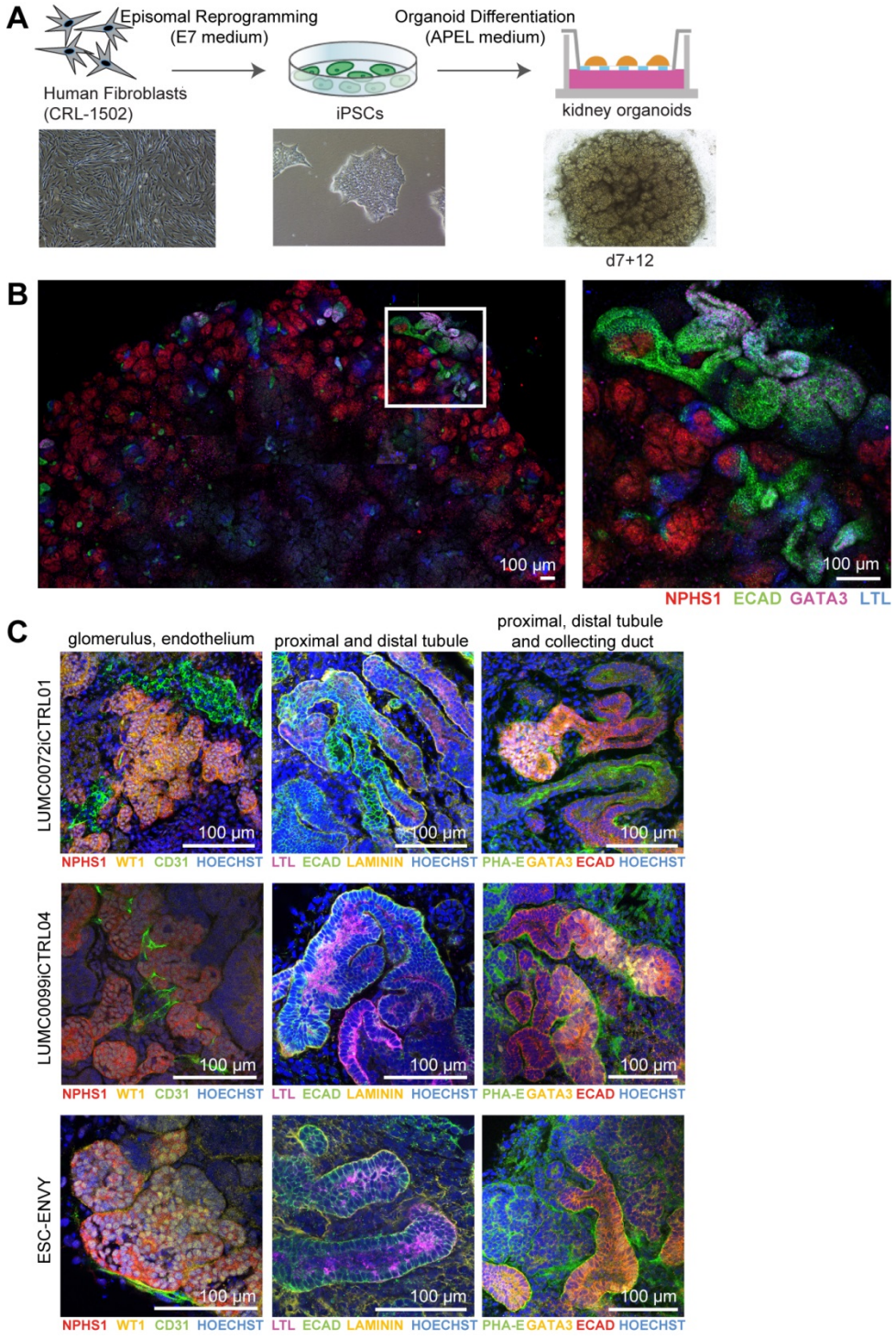

Figure S2: Human Kidney Organoids Derived from Multiple Pluripotent Stem Cell Lines Contain All Nephron Structures

(A) Kidney organoids can be derived from hiPSCs that were originally generated by episomal reprogramming of human fibroblasts in Essential 7 (E7) medium without culture on mouse embryonic fibroblasts.

(B) Tile scan of a kidney organoid generated from hiPSCs derived in E7 medium displays all characteristic compartments of a nephron: glomerulus ($NPHS1^+$), proximal (LTL^+) and distal tubular ($ECAD^+$) segments and collecting duct ($GATA3^+$) on day 7 + 12 of differentiation. Close-up view of the boxed area displays the structures in detail.

(C) Kidney organoids derived from one additional embryonic (ESC-ENVY) and two induced pluripotent stem cell lines (LUMC0072iCTRL01 and LUMC0099iCTRL04) display characteristic glomerular structures ($NPHS1^+$, $WT1^+$), endothelial cells ($CD31^+$), proximal tubules ($PHA\text{-}E^+$, LTL^+), distal tubules ($ECAD^+$) and collecting duct ($GATA3^+$) on day 7 + 18.

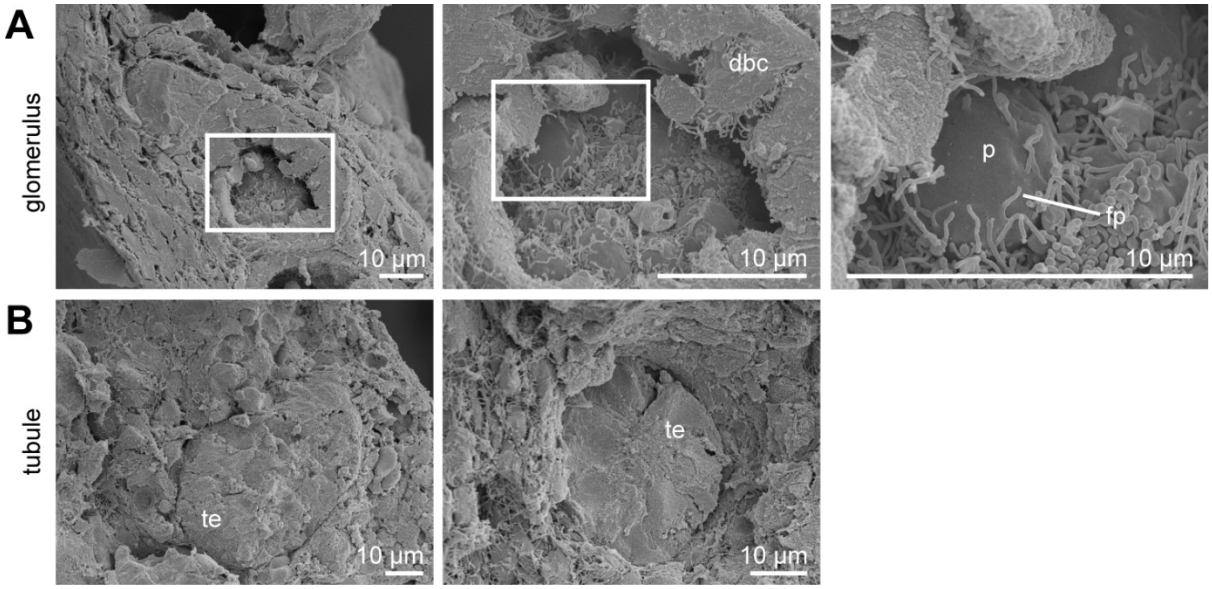

Figure S3: Scanning Electron Microscopy (SEM) Analysis of Kidney Organoids on Day 7 + 18
(A) Developing Bowman's capsule is surrounding the glomerular structure. Boxed areas show close-up views of the glomerular structure and podocytes with primitive foot processes.
(B) SEM showing tubular structures in kidney organoid.
dbc, developing Bowman's capsule; p, podocytes; fp, foot processes; te, tubular epithelium.

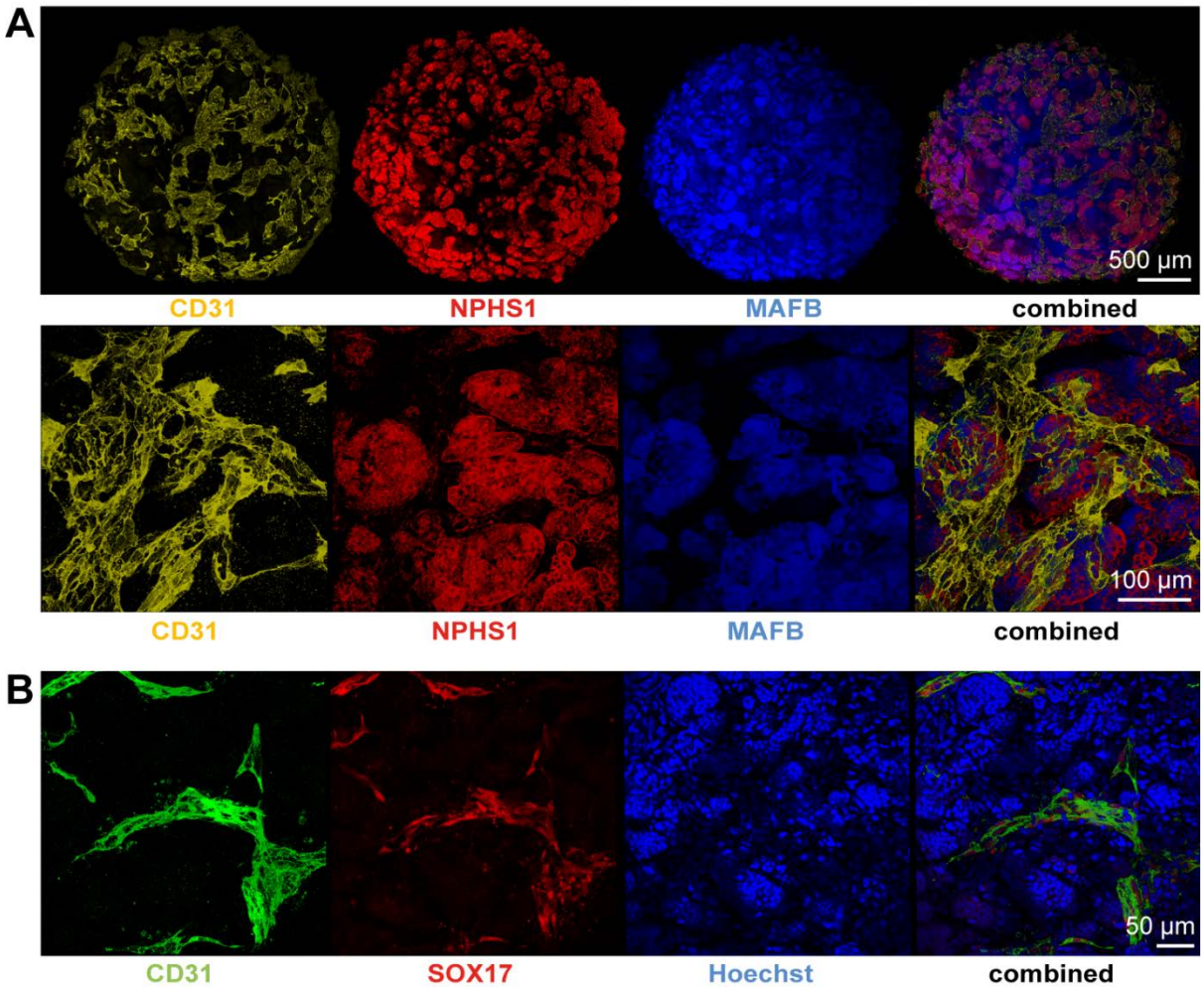

Figure S4: Characterisation of Kidney Organoids Derived from hiPSC-MAFB-BFP and hESC-SOX17-mCherry Reporter Lines
(A) Kidney organoids derived from hiPSC-MAFB-BFP reveal co-localisation of $NPHS1^{+}$ and mTagBFP2 reporter expression in the podocyte population in developing glomeruli surrounded by $CD31^{+}$ endothelial cells. **(B)** hESC-SOX17-mCherry derived kidney organoids display co-localisation of $CD31^{+}$ endothelial cells and SOX17-$mCherry^{+}$ cells.

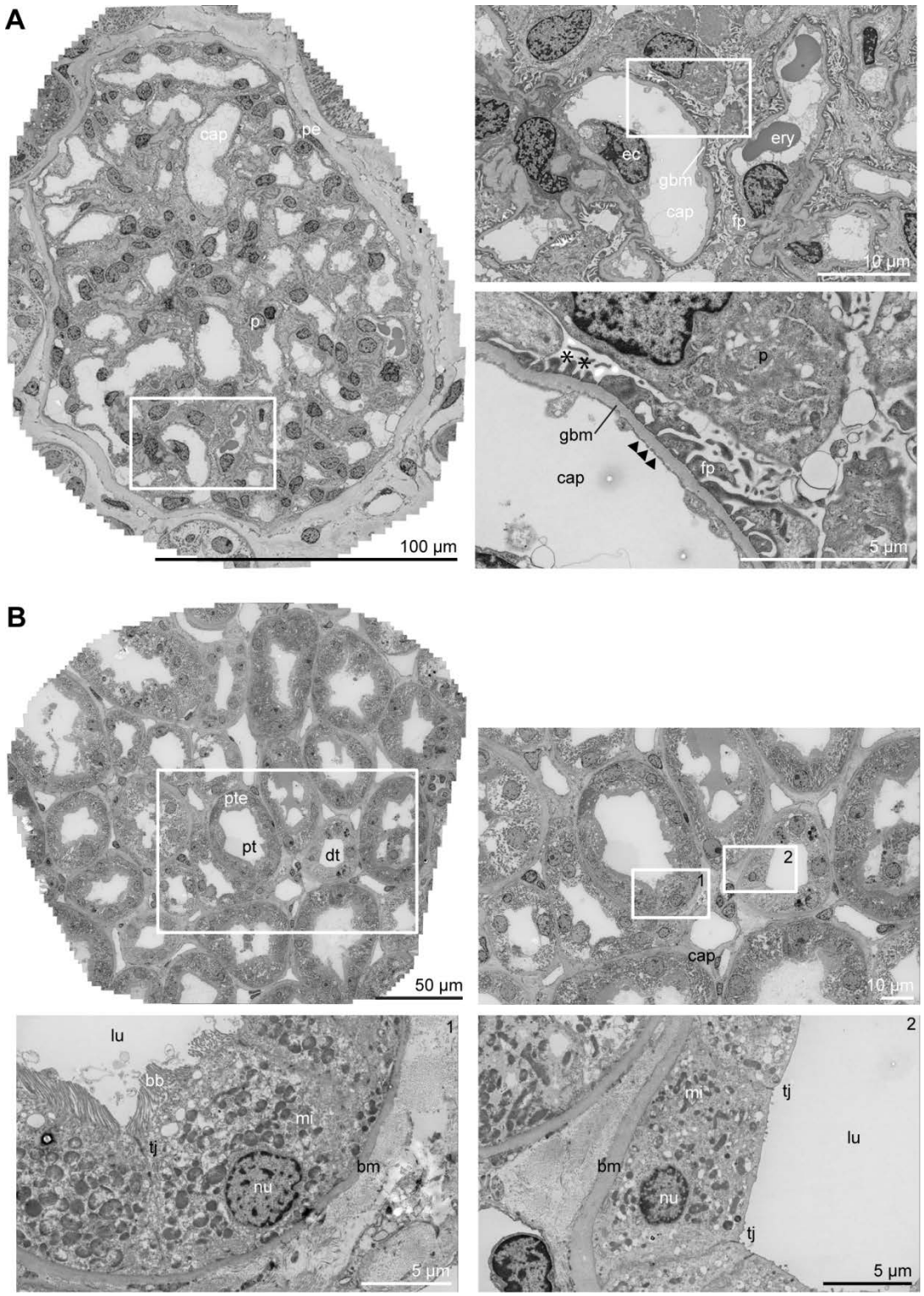

Figure S5: Ultrastructural Reference of Glomerulus and Tubular Structures in the Human Kidney
(A) Transmission electron microscopy overview of a glomerulus with boxed areas displaying close-up views of the glomerular structure and foot processes. Boxed areas correspond with close-up views.
(B) Various cortical tubular structures in a human kidney. Numbered boxed areas display close up views of distinct tubular structures.
p, podocytes; cap, capillary; pe, parietal epithelium; ec, endothelial cell; ery, erythrocyte; fp, foot process; gbm, glomerular basement membrane; asterisk, slit diaphragm; arrow head, fenestrae; pte, proximal tubular epithelium; pt, proximal tubule; dt, distal tubule; lu, lumen; bb, brush border; mi, mitochondria; nu, nucleus; bm, basement membrane; tj, tight junction.

Movie S1:
***In Vivo* Imaging (z Stack) of Vascularized hiPSC-MAFB-BFP Organoids after Labelling of Blood Plasma with 2,000 kDA FITC-labelled Dextran after 7 and 14 Days of Transplantation**

Movie S2:
***In Vivo* Imaging (z Stack) of Vascularized hESC-SOX17-mCherry Organoids after Labelling of Blood Plasma with 2,000 kDA FITC-labelled Dextran after 14 Days of Transplantation**

Supplemental Experimental Procedures

Maintenance of Human Pluripotent Stem Cells

hESC and hiPSC lines were maintained in Essential 8 medium (E8, Thermo Fisher Scientific) according to the manufacturers protocol. hESC-ENVY (Costa et al., 2005), H9 hESC line *SOX17*$^{mCHERRY/w}$*RUNX1C*$^{GFP/w}$ (hESC-SOX17-mCherry) (Ng et al., 2016) and hiPSC-CRL1502 clone C32 (Briggs et al., 2013) were initially maintained on irradiated mouse embryonic feeders (MEFs) and hESC medium (Costa et al., 2008) before transfer to feeder free culture conditions.

Also numerous other hiPSC lines were investigated. An extra hiPSC-CRL1502 line was generated without the use of MEFs using episomal reprogramming plasmids (Chen et al., 2011) including a plasmid encoding miR302-367 (Howden et al., 2015) and mRNA encoding a truncated version of EBNA1 (Chen et al., 2011). Electroporation was performed using a Neon Transfection Device (Thermo Fisher Scientific) (1,400 V, 20 ms, 2 pulses). Cells were initially maintained in fibroblast medium (DMEM/F12 (Thermo Fisher Scientific) supplemented with 15% FCS and 1× NEAA (Thermo Fisher Scientific)) followed by E7 medium (Essential 8 medium without transforming growth factor β) and further cultured in E8 medium using EDTA for passaging. Reporter hiPSC *MAFB*:mTagBFP2 (hiPSC-MAFB-BFP) was simultaneously reprogrammed and gene-edited using CRISPR/Cas9 in E8 medium (unpublished).

Two other hiPSC lines, LUMC0072iCTRL01 and LUMC0099iCTRL04, were generated on MEFs from fibroblasts using Simplicon RNA Reprogramming Kit (Millipore) (iPSC core facility, LUMC) and further cultured in TeSR-E8 medium (Stem Cell Technologies). Pluripotency and spontaneous differentiation to the three germlayers was verified by immunofluorescence. All cell lines were negative for mycoplasma. All hiPSCs were transferred to culture in E8 medium on vitronectin and were maintained for several passages as small clumps using 0.5 mM UltraPure EDTA (Thermo Fisher Scientific) before transfer to E8 culture as single cells using TrypLE Select (Thermo Fisher Scientific) and the addition RevitaCell Supplement (ThermoFisher Scientific) for 24 hr. The E8 medium was supplemented with 0.5% Penicillin-Streptomycin (Thermo Fisher Scientific) and hPSCs were passaged twice a week.

Differentiation and Organoid Formation

hPSCs were plated for differentiation on vitronectin coated culture dishes at 10,000 cells / cm^2 in E8 medium supplemented with RevitaCell. The cells were cultured until the dish was about 10–20% confluent (usually 24 hr) on the day that the differentiation was started (day 0). Cells were incubated for 4 days in 8 μM CHIR99021 (R&D Systems) in STEMdiff APEL medium (APEL) or STEMdiff APEL2 medium (Stem Cell Technologies) supplemented with 1% Protein Free Hybridoma Medium II (PFHMII, Thermo Fisher Scientific) and Antibiotic-Antimycotic (Thermo Fisher Scientific). From day 4–7, cells were treated with 200 ng mL^{-1} rhFGF9 (R&D Systems) and 1 μg mL^{-1} heparin (Sigma Aldrich) in APEL medium. After 7 days, cells were switched from monolayer culture to 3D culture after a 1 hr pulse with 5 μM CHIR to stimulate nephrogenesis. Differentiated cells were dissociated using Trypsin-EDTA (0.25%, Thermo Fisher Scientific) and centrifuged at 400 × *g* containing 500,000 cells per tube. The pellets were transferred to a Transwell 0.4 μM pore polyester membrane and further cultured on an air-liquid interface for another 5 days in APEL medium containing 200 ng mL^{-1} rhFGF9 and 1 μg mL^{-1} heparin (only bottom compartment). For the remaining days, the organoids were further cultured in medium without FGF9 and heparin and medium was changed every 2 days. Organoids were maintained on the transwell membranes until day 7 + 18 to day 7 + 53.

Animal Experiments

All animal experimental protocols were approved by the animal welfare committee of the Leiden University Medical Center. Eight week old recipient mice (n = 8, non-obese diabetic/severe combined immunodeficiency (NOD/SCID), Charles River Laboratories) were anesthetized with isoflurane and injected with temgesic (buprenorphine) for pain relief before surgery. Core body temperature was maintained at 37 °C. Via flank incisions, the kidneys were exteriorized and a small incision was made in the renal capsule. Kidney organoids, cultured for 7 + 18 days were bisected and transplanted under renal capsule in the left and right kidney. The mice were anesthetized and sacrificed after 7 and 28 days and the kidneys were collected.

Intravital Microscopy

For Intravital microscopy, 8 week old recipient mice (n = 10, NOD/SCID, Charles River Laboratories) were anesthetized with isoflurane and injected with temgesic (buprenorphine) for pain relief before surgery. Core body temperature was maintained at 37 °C. Organoids derived from hiPSC-MAFB-BFP and hESC-SOX17-mCherry were transplanted under the renal capsule as described above. A titanium abdominal imaging window was implanted on top of the left kidney as described (Ritsma et al., 2012; van Gurp et al., 2016). In short, a purse-string suture was placed in the intra-abdominal muscle, the kidney was exposed and then fixed in the subcutaneous space by tightening of the suture around the stalk while blood flow and ureter remained intact. A second purse-string suture was made along the edge of the incision in the skin and an abdominal window was fitted, placing the skin in the window groove. Tightening the suture fixed the window in the skin with the kidney and organoid directly underneath it. After surgery, mice were housed separately and provided with food and water at libitum. Seven and 14 days after surgery the mice were intravitally imaged on a Zeiss LSM 710 NLO upright multiphoton microscope equipped with a tunable Mai Tai Deep See multiphoton laser (690–1040 nm). Mice were anesthetized with isoflurane and their core body temperature was kept at 37 °C during the imaging session using a temperature-controlled heat mat connected to a rectal probe. Mice were intravenously injected in the tail vein with 2,000 kDa FITC-Dextran (100 µL of 20 mg/mL, Sigma FD2000S) before the imaging started. The animals were placed on their side on a custom-made microscope insert with the window stably fixed in an upward horizontal position using a custom made window holder. Imaging was performed through a W Plan-Apochromat 20×/1.0 DIC M27 75 mm objective. Fluorophores in iPSC-MAFB-BFP organoids were excited at 800 nm and emission was collected in two LSM PMTs: FITC (522–600 nm) and BFP (440–500 nm). Fluorophores in hESC-SOX17-mCherry organoids were excited using single photon at 488 (FITC) and 568 (mCherry) and emission was collected in two LSM PMTs: FITC (500–558 nm) and mCherry (578–700 nm). Time lapse series were collected and Z stacks were taken with a Z-step of 1 or 2 µm.

Immunohistochemistry

Organoids (day 7 + 18) were stained for kidney structures as described previously (Takasato et al., 2015, 2016). Briefly, organoids were fixed in 2% paraformaldehyde (PFA) at 4 °C for 20 minutes. The organoids were permeabilized and blocked in 10% donkey serum in 0.3% TritonX in PBS for 2 hr. Primary antibodies were incubated overnight and were detected by secondary antibodies incubated for 2 hr at room temperature or overnight at 4 °C. Organoids under the mouse renal capsule were snapfrozen in TissueTek or fixed for 20 min in 2% PFA and stored in PBS for whole mount analysis. Frozen kidney sections (5–10 µm thick) were fixed in 2% PFA for 10 minutes at room temperature and permeabilized in 0.3% TritonX in PBS for 15 minutes. Mouse on Mouse Basic Kit was used to detect structures in the human organoid and mouse kidney.
Immunofluorescence characterisation of the transplanted and non-transplanted organoids was performed using antibodies for NPHS1 (AF4269, R&D Systems), WT1 (SC-192, Santa Cruz Biotechnology), CUBILIN (SC-20607, Santa Cruz Biotechnology), CD31 (555444, BD Biosciences), ECAD (610181, BD Biosciences), MECA-32 (553849, BD Biosciences), LTL-biotin-conjugated (B-1325, Vector Laboratories), FITC-conjugated PHA-E (FL-1121, Vector Laboratories), Tamm Horsfall (BT85-9500-54, Biotrend) thiazide-sensitive NaCl cotransporter (NCC, AB3553, Millipore), aquaporin-2 (AQP2) (kindly provided by Joost Hoenderop and Peter Deen, Nijmegen), GATA3 (AF2605, R&D Systems), PDGFR-β (MAB1263, R&D Systems), MEIS1/2/3 (39795, Active Motif), LAMININ (L9393, Sigma Aldrich) and human nuclei (abin361360, antibodies-online). Primary antibodies were detected with donkey-α-sheep Alexa Fluor 568 (A-21099) and 647 (A-21448), donkey-α-rabbit Alexa Fluor 568 (A-10042) and 647 (A-31573), donkey-α-mouse Alexa Fluor 488 (A-21202), goat-α-mouse Alexa Fluor 488 (A-21121), donkey-α-goat Alexa Fluor 568 (A-11057) and 647 (A-21447), donkey-α-rat Alexa Fluor 488 (A-21208), goat-α-guinea pig Alexa Fluor 647 (A-21450), streptavidin Alexa Fluor 532 (S11224, all Thermo Fisher Scientific) and donkey-α-rat Alexa Fluor 568 (ab175475, Abcam).
Organoids and sections were counterstained with Hoechst33258 (Thermo Fisher Scientific) and embedded in ProLong Gold Antifade Mountant (Thermo Fisher Scientific) respectively in 35 mm glass bottom dishes (MatTek corporation) or adhesive microscope slides (StarFrost, Knittel glass). Tissues were examined using the Leica White Light Laser Confocal Microscope TCS SP8 using LAS-X Image software with 3D module (Leica) or the LSM 780 confocal microscope (Zeiss).

Cytokine Analysis

Cell culture supernatant of the organoids was collected weekly from day 7 + 10 until day 7 + 52 from 1 to 3 wells with 3 organoids during 3 independent differentiations. The levels of VEGF released into the supernatant were assessed using the Human Premixed Magnatic Luminex Assay for VEGF according to the manufacturer's protocol. The Bio-Plex Luminex system (Bio-Rad) was used for readout and VEGF concentration was expressed as pg mL^{-1}.

Transmission and Scanning Electron Microscopy

Tissue samples of organoids at day 7 + 18 and organoids under the mouse renal capsule were fixed overnight at 4 °C in 1.5% glutaraldehyde (Electron Microscopy Sciences) in 0.1 M sodium-cacodylate buffered solution, pH 7.4. Subsequently, the tissue was rinsed twice with 0.1 M sodium cacodylate-buffered solution, and fixed for 1 hr on ice in 1% osmium tetroxide (Electron Microscopy Sciences) in sodium cacodylate buffer. Tissue probes were further washed 2× with sodium cacodylate buffer, dehydrated overnight in 70% ethanol, then in 80% ethanol (10 min), 90% ethanol (10 min), and 100% ethanol absolute (twice 15 min; once 30 min).

For TEM, the tissue samples were further infiltrated with a mixture of epon LX-112 (Ladd Research) and propylene oxide (Electron Microscopy Sciences) (1:1) for 1 hr, followed by pure epon for 2 hr, embedded in pure epon, mounted in BEEM capsules (Agar Scientific) and polymerized for 48 hr at 60 °C. Ultrathin sections (100 nm) were mounted on copper slot grids (Storck Veco B.V.), covered with formvar film and carbon layer, and then stained with an aqueous solution of 7% uranyl acetate for 20 minutes, followed by Reynold's lead citrate for 10 minutes. Organoids at day 7 + 18 and organoids under the mouse renal capsule were analyzed at an acceleration voltage of 120 kV using an FEI Tecnai 12 (BioTWIN) transmission electron microscope (FEI), equipped with an FEI 4k Eagle CCD camera. Virtual slides showing glomerular and tubular structures that allow for an unbiased assessment of the whole organoids were recorded using automated large-scale data acquisition combined with stitching software (Faas et al., 2012). Images were captured at 13,000× or 18,500× magnification, respectively corresponding to a 1.66 or 1.22 nm pixel size at the specimen level.

For SEM, dehydration of the tissue samples was immediately followed by critical point drying. Samples were mounted on 0.5" SEM pin stubs (Agar Scientific) covered with conductive carbon discs (Agar Scientific) and then coated with gold-palladium. SEM images were acquired on a JEOL JSM-6700F Field Emission Scanning Electron Microscope (JEOL Europe B.V.).

References in Supplemental Experimental Procedures

Briggs, J.A., Sun, J., Shepherd, J., Ovchinnikov, D.A., Chung, T.L., Nayler, S.P., Kao, L.P., Morrow, C.A., Thakar, N.Y., Soo, S.Y., *et al.* (2013). Integration-free induced pluripotent stem cells model genetic and neural developmental features of down syndrome etiology. Stem Cells *31*, 467-478.

Chen, G., Gulbranson, D.R., Hou, Z., Bolin, J.M., Ruotti, V., Probasco, M.D., Smuga-Otto, K., Howden, S.E., Diol, N.R., Propson, N.E., *et al.* (2011). Chemically defined conditions for human iPSC derivation and culture. Nat Methods *8*, 424-429.

Costa, M., Dottori, M., Ng, E., Hawes, S.M., Sourris, K., Jamshidi, P., Pera, M.F., Elefanty, A.G., and Stanley, E.G. (2005). The hESC line Envy expresses high levels of GFP in all differentiated progeny. Nat Methods *2*, 259-260.

Costa, M., Sourris, K., Hatzistavrou, T., Elefanty, A.G., and Stanley, E.G. (2008). Expansion of human embryonic stem cells in vitro. Curr Protoc Stem Cell Biol *5:C*, 1C.1.1–1C.1.7.

Faas, F.G., Avramut, M.C., van den Berg, B.M., Mommaas, A.M., Koster, A.J., and Ravelli, R.B. (2012). Virtual nanoscopy: generation of ultra-large high resolution electron microscopy maps. J Cell Biol *198*, 457-469.

Howden, S.E., Maufort, J.P., Duffin, B.M., Elefanty, A.G., Stanley, E.G., and Thomson, J.A. (2015). Simultaneous Reprogramming and Gene Correction of Patient Fibroblasts. Stem Cell Reports *5*, 1109-1118.

Ng, E.S., Azzola, L., Bruveris, F.F., Calvanese, V., Phipson, B., Vlahos, K., Hirst, C., Jokubaitis, V.J., Yu, Q.C., Maksimovic, J., *et al.* (2016). Differentiation of human embryonic stem cells to HOXA(+) hemogenic vasculature that resembles the aorta-gonad-mesonephros. Nat Biotechnol *34*, 1168-1179.

Ritsma, L., Steller, E.J., Beerling, E., Loomans, C.J., Zomer, A., Gerlach, C., Vrisekoop, N., Seinstra, D., van Gurp, L., Schafer, R., *et al.* (2012). Intravital microscopy through an abdominal imaging window reveals a pre-micrometastasis stage during liver metastasis. Science translational medicine *4*, 158ra145.

Takasato, M., Er, P.X., Chiu, H.S., and Little, M.H. (2016). Generation of kidney organoids from human pluripotent stem cells. Nat Protoc *11*, 1681-1692.

Takasato, M., Er, P.X., Chiu, H.S., Maier, B., Baillie, G.J., Ferguson, C., Parton, R.G., Wolvetang, E.J., Roost, M.S., Chuva de Sousa Lopes, S.M., *et al.* (2015). Kidney organoids from human iPS cells contain multiple lineages and model human nephrogenesis. Nature *526*, 564-568.

van Gurp, L., Loomans, C.J.M., van Krieken, P.P., Dharmadhikari, G., Jansen, E., Ringnalda, F., Beerling, E., van Rheenen, J., and de Koning, E.J.P. (2016). Sequential intravital imaging reveals in vivo dynamics of pancreatic tissue transplanted under the kidney capsule in mice. Diabetologia *59*, 2387-2392.